Multiple reservoirs of volatiles in the Moon revealed by the isotopic composition of chlorine in lunar basalts

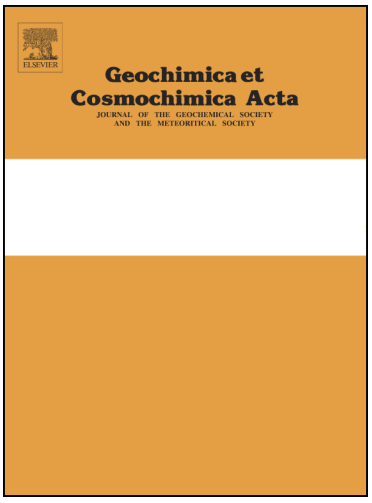

Multiple reservoirs of volatiles in the Moon revealed by the isotopic composition of chlorine in lunar basalts

Jessica J. Barnes, Ian A. Franchi, Francis M. McCubbin, Mahesh Anand

PII: S0016-7037(18)30720-8
DOI: https://doi.org/10.1016/j.gca.2018.12.032
Reference: GCA 11065

To appear in: *Geochimica et Cosmochimica Acta*

Received Date: 21 May 2018
Revised Date: 15 December 2018
Accepted Date: 20 December 2018

Please cite this article as: Barnes, J.J., Franchi, I.A., McCubbin, F.M., Anand, M., Multiple reservoirs of volatiles in the Moon revealed by the isotopic composition of chlorine in lunar basalts, *Geochimica et Cosmochimica Acta* (2018), doi: https://doi.org/10.1016/j.gca.2018.12.032

Multiple reservoirs of volatiles in the Moon revealed by the isotopic composition of chlorine in lunar basalts

Jessica J. Barnes[1,2,3], Ian A. Franchi[1], Francis M. McCubbin[2], & Mahesh Anand[1,4]

[1]School of Physical Sciences, The Open University, Walton Hall, Milton Keynes, MK7 6AA, U.K.
[2]ARES, NASA Johnson Space Center, Houston, Texas, 77058, U.S.A.
[3]Lunar and Planetary Laboratory, University of Arizona, Tucson, Arizona, 85721, U.S.A
[4]Department of Earth Sciences, Natural History Museum, London, U.K
Email correspondence: jessica.j.barnes@nasa.gov jjbarnes@lpl.arizona.edu

Abstract

The isotopes of chlorine (^{37}Cl and ^{35}Cl) are highly fractionated in lunar samples compared to most other Solar System materials. Recently, the chlorine isotope signatures of lunar rocks have been attributed to large-scale degassing processes that occurred during the existence of a magma ocean. In this study we investigated how well a suite of lunar basalts, most of which have not previously been analyzed, conform to previous models. The Cl isotope compositions (δ^{37}Cl (‰) = [(^{37}Cl/^{35}Cl$_{sample}$/^{37}Cl/^{35}Cl$_{SMOC}$)-1]×1000, where SMOC refers to standard mean ocean chloride) recorded range from ~+7 to +14 ‰ (Apollo 15), +10 to +19 ‰ (Apollo 12), +9 to +15 ‰ (70017), +4 to +8 ‰ (MIL 05035), and +15 to +22 ‰ (Kalahari 009). The Cl isotopic data from the present study support the mixing trends previously reported by Boyce et al. (2015) and Barnes et al. (2016), as the Cl isotopic composition of apatites are positively correlated with bulk-rock incompatible trace element abundances in the low-Ti basalts, inclusive of low-Ti and KREEP basalts. This trend has been interpreted as evidence that incompatible trace elements, including Cl, were concentrated in the urKREEP residual liquid of the lunar magma ocean, rather than the mantle cumulates, and that urKREEP Cl had a highly fractionated isotopic composition. The source regions for the basalts were thus created by variable mixing between the mantle (Cl-poor and relatively unfractionated) and urKREEP. The high-Ti basalts show much more variability in measured Cl isotope ratios and scatter around the trend formed by the low-Ti basalts. Most of the data for lunar meteorites also fits the mixing of volatiles in their sources, but Kalahari 009, which is highly depleted in incompatible trace elements, contains apatites with heavily fractionated Cl isotopic compositions. Given that Kalahari 009 is one of the oldest lunar basalts and ought to have been derived from very early-formed mantle cumulates, a heavy Cl isotopic signature is likely not related to its mantle source, but more likely to magmatic or secondary alteration processes, perhaps via impact-driven vapor metasomatism of the lunar crust.

Keywords

Apatite, NanoSIMS, isotope fractionation, Apollo samples, lunar meteorites

1. Introduction

One of the recent breakthroughs in Solar System volatiles research has been the demonstration that the chemical properties of apatite, a calcium phosphate mineral with the formula $Ca_5(PO_4)_3(F,Cl,OH)$, make it a robust and versatile mineral with which to trace the volatile history of magmatic systems. Apatites occur in basalts and granites (or granite-like compositions) from numerous differentiated and undifferentiated planetary bodies, including the Earth (e.g., McConnell, 1973; Boudreau and Simon, 2007; Chu et al., 2009), the Moon (e.g., Papike et al., 1991; Boyce et al., 2010; McCubbin et al., 2010a; Greenwood et al., 2011), Mars (e.g., McSween, 1994; Hallis et al., 2012; McCubbin et al., 2013; McCubbin et al., 2016), the asteroid 4-Vesta (Mittlefehldt et al., 1998; Sarafian et al., 2013), and on L, LL, and H ordinary chondrite parent bodies (e.g., Brearley and Jones, 1998; Jones et al., 2014; Jones et al., 2016; Lewis and Jones, 2016). Planetary apatite varies from sub-micron to hundreds of microns in the longest dimension (McCubbin and Jones, 2015), and host variable amounts of F, Cl, and OH in its crystal structure as essential structural constituents (ESCs) (review by Hughes and Rakovan, 2015). In fact, in some rocks such as those from the Moon, apatite is the most common OH-bearing mineral, occurring in a variety of lithologies (see review by McCubbin et al., 2015b). The presence of volatiles in apatite coupled with its common occurrence in planetary materials has motivated numerous studies to develop apatite as a magmatic hygrometer in planetary systems (Boyce et al., 2014; Li and Hermann, 2015; McCubbin et al., 2015a; Li and Hermann, 2017; Mccubbin and Ustunisik, 2018; Riker et al., 2018), provided it is utilized in a suitable manner (Boyce et al., 2014). Since apatite harbors OH and Cl in its crystal structure, it is particularly useful for studies of the stable isotopes of H and Cl. These ratios can reveal the source(s) of volatiles in the terrestrial planets and asteroids and variations among and between different objects can tell us about the variety of magmatic and secondary processes that have operated.

Of interest to us is chlorine, as it is an incompatible, moderately volatile, and hydrophilic element making it an important tracer of hydrous activity and evaporation processes. The isotopic composition of chlorine is reported as $\delta^{37}Cl$ (‰) = $[(^{37}Cl/^{35}Cl_{sample}/^{37}Cl/^{35}Cl_{SMOC})-1]\times1000$, where SMOC refers to standard mean ocean chloride with a composition of 0 ‰ (Kaufmann et al., 1984). The isotopes of Cl have been measured in volcanic rocks, metamorphic rocks, sedimentary rocks, and evaporite deposits on Earth (e.g., Sharp et al., 2007; Barnes et al., 2008; Barnes et al., 2009) as well as in bulk carbonaceous and ordinary

chondrites (Sharp et al., 2007; Sharp et al., 2013b), showing variation from ~-5 to +5 ‰ (reviewed by Barnes and Sharp, 2017). Chlorine isotopes in meteorites from differentiated bodies outside the Earth-Moon system are characterized by compositions in the range of ~-4 to +10 ‰ (Sharp et al., 2016; Williams et al., 2016; Bellucci et al., 2017; Sarafian et al., 2017; Shearer et al., 2018). For martian rocks, such excursions from unfractionated Cl isotopic compositions have been linked to crustal/fluid assimilation (e.g., Shearer et al., 2018). On the HED parent-body, positive δ^{37}Cl values of up to ~12 ± 1 ‰ measured in eucrites have been linked to Rayleigh degassing of metal chlorides and HCl from an early magma ocean (Sarafian et al., 2017). Presently, the Moon is the only planetary body for which even greater fractionations have been observed, generally up to ~+30 ‰ (Sharp et al., 2010a; Shearer et al., 2014; Tartèse et al., 2014a; Treiman et al., 2014; Boyce et al., 2015; Barnes et al., 2016; Potts et al., 2018), but in one meteorite up to ~+81 ‰ (Wang et al., 2012) (Figure 1).

The range of Cl isotopes from ~-4 to ~+30 ‰ in many lunar samples have been linked to the global differentiation of the Moon via the so-called lunar magma ocean (LMO) (Smith et al., 1970; Wood et al., 1970). In that model, the final melts in the interior were concentrated in incompatible trace elements (ITEs), including volatiles, which were not incorporated into the minerals that had previously crystallized to form the mantle and crust of the Moon. These final vestiges of melt are referred to as urKREEP in its primitive form or KREEP as a geochemical component implying that it was derived from urKREEP proper (Warren and Wasson, 1979). Boyce et al. (2015) showed that a positive correlation exists between the Cl isotopic composition of lunar apatites and bulk-rock ITE abundances for lunar basalts of different bulk compositions (i.e., KREEP basalts, and high and low-Ti basalts). Barnes et al. (2016) confirmed and extended this same trend through the investigation of a diverse suite of samples that included a very high potassium basalt and several ancient (> 3.9 Ga) samples of the lunar highlands magnesian suite. Barnes et al. (2016) hypothesized that the observed correlations between Cl isotopic composition and bulk-rock ITE abundances may be a unique feature of rocks within the Procellarum KREEP Terrane (PKT) that could be related to the formation of the PKT region of the lunar nearside rather than a global-scale event. However, they pointed out that additional Cl isotope data, especially on samples from regions away from the PKT region, as well as those not represented in the Apollo and Luna collections, were needed to assess this hypothesis. Each of these models rely heavily on limited data from few low-Ti basalts. In this study we sought to more thoroughly test these hypotheses, by investigating the Cl isotopic compositions and volatile inventories of a suite of low-Ti basalts from several Apollo missions. We also studied two meteorites, one of very-low-Ti (VLT) and one of low-Ti basaltic compositions that have variable ITE contents. In

particular, the VLT basalt (Kalahari 009) is thought to have originated from the lunar farside. Our data confirm that lunar basalts contain fluorapatites that display a wide range of Cl isotope compositions. We show that the Apollo basalts, regardless of composition, agree with the current models forwarded for the evolution of Cl in the Moon (forwarded by Boyce et al., 2015). The basaltic lunar meteorites represent a random sampling of lunar lithologies and provide insights into the various reservoirs of Cl in the Moon. These data enable further evaluation of the extent, timing, and scale of Cl isotopic fractionation processes on the Moon.

2. NanoSIMS methods

The Cameca NanoSIMS 50L at The Open University was used to analyze the isotopic and chemical compositions of volatiles in apatites in the diverse suite of lunar basalts to provide insight into the origin of extensive isotopic fractionation of Cl on the Moon. An amended analytical protocol after Barnes et al. (2016) was used to measure Cl isotopes and Cl, H_2O, and F abundances of the apatites. (Note that whilst molecular OH^- is present in the apatite crystal structure, henceforth we will refer to the equivalent amount of H_2O). We also analyzed the D/H ratio and H_2O content of some lunar apatites by NanoSIMS.

2.1. Standards

This study utilized terrestrial apatite crystals that are typically used as reference materials for volatile analyses by several groups (McCubbin et al., 2012; Barnes et al., 2014; McCubbin et al., 2015a; Robinson et al., 2016). The apatite crystals used include Ap003 from Durango in Mexico, Ap004 from the Atlas Mountains of Morocco, Ap005 from the Crystal Lode Pegmatite Mine in Colorado, U.S.A, and Ap018 from Lake Baikal, Slyudyanka in Russia (described by McCubbin et al., 2010; McCubbin et al., 2012). The isotopic compositions were generally referenced to Ap004 with a Cl isotopic composition of +0.1 ‰, as determined by Z. Sharp at University of New Mexico using an isotope ratio mass spectrometer (Barnes et al., 2016; Potts et al., 2018). All samples and standards were gold coated (30 nm thick) prior to NanoSIMS analysis.

2.2. Detailed analytical protocol

The NanoSIMS 50L ion probe was used in multi-collection mode during an analytical session in February 2016. A primary Cs+ ion beam of ~30 pA and <1 µm diameter was accelerated with a voltage of ~8kV. The negative secondary ions of $^{16}O^1H$, ^{18}O, ^{19}F, ^{35}Cl, and ^{37}Cl were collected simultaneously in electron multipliers (EM). Count rates of ^{18}O were monitored and treated as an internal reference. Cracks were easily identified based on

correlated highs of OH and Cl ions in isotope imaging mode. An F-bearing molecular ion was monitored on EM #7 (at mass 59) to locate apatite using real-time isotope imaging. The mass spectrometer was tuned to a mass resolving power of ~9000 (Cameca definition), sufficient enough to resolve any isobaric interferences between $^{16}O^{1}H$ and ^{17}O. The incident ion beam was rastered over 10 µm × 10 µm areas during pre-sputtering and over smaller areas typically ~5 µm × 5 µm during analysis. Prior to analysis, pre-sputtering was performed using ~100 pA probe for ~2 minutes, and then the secondary ion beam was aligned both horizontally and vertically in the entrance slit. A total of 500 measurements were collected per each 8-minute analysis. For apatite standards, multiple analyses of a single crystal were made in isotope analysis mode as chains with the sputtered ion beam being automatically centered before each analysis through the immersion lens and deflector plates. Mass scans of ^{18}O and ^{35}Cl were performed automatically during each analysis. Electronic gating was not employed. Note that multiple sample exchanges were necessary during the main analytical session due to a limited number of sample holders.

Apatite can contain up to 3.77 wt.% F (at an end-member composition, fluorapatite). Often the F-rich nature of lunar apatites resulted in sputter ion yields exceeding 1 million counts arriving at EM #4, which can significantly contribute to aging of the detector, thereby limiting its usable lifetime. Therefore, the secondary ion beam arriving at EM #4 was deflected during most of the initial instrument tuning by using ~8 V deflection applied to the electrostatic deflector positioned in front of EM #4. During each analysis, the on-peak signal was measured every 50 frames for ~8 seconds.

We used apatite standards that were mounted in Lakeside resin from Agar Scientific Ltd. in 10 mm round brass rings and polished flat with a flush contact achieved between the apatites and epoxy. We mounted the apatites in the resin to limit any potential topographic issues introduced by pressing the samples into indium metal. The volatile (Cl, H_2O, and F) abundances of the lunar apatites were calculated by calibrating the measured ratios on the standards against their reported concentrations (i.e., McCubbin et al., 2012) (further calibration details can be found in the Electronic Annex). The instrumental background contribution of H_2O to the measurements was assessed using an epoxy-mounted nominally anhydrous San Carlos olivine crystal and varied from ~100-650 ppm across the analytical session (Electronic Annex). In addition, nominally anhydrous minerals, usually pyroxene, were analyzed in some of the studied lunar thin sections with comparable measured values (Table A.2). Compared to studies dedicated to the measurement of H_2O or D/H ratios (e.g., Barnes et al., 2014), the reported H_2O backgrounds here are somewhat higher (Table A.1). This could be related to (i) mounting the standards in epoxy rather than indium, (ii) the low primary beam currents used, (iii) multiple sample exchanges during the analytical session, or

(iv) not employing electronic gating during measurements. In apatites with relatively high H_2O contents (>1000 ppm H_2O), like those in 15065, the background makes up less than 15% of the total measured H_2O providing confidence the values reported are robust. In contrast for a few apatites with <200 ppm H_2O, such as from 70017, the H_2O data associated with Cl isotope measurements should be treated with caution as the H_2O background comprises the majority of, if not all, of the total measured H_2O.

2.3. Results on primary and secondary standards

Ap004 (0.41 wt.% Cl) was used as a primary reference standard for most lunar samples. To correct the measured $^{37}Cl/^{35}Cl$ ratios on secondary standards and the majority of lunar apatites for instrumental mass fractionation (IMF) a reference apatite was used, Ap004 ($\delta^{37}Cl$ = +0.11 ‰). For Ap004, the IMF (defined as [($^{37}Cl/^{35}Cl_{measured}/^{37}Cl/^{35}Cl_{true}$-1) ×1000]) was +19 ± 6 ‰ (n = 40). The typical reproducibility of $^{37}Cl/^{35}Cl$ ratio on Ap004 was generally better than 1 ‰ the uncertainty represents the 2 standard deviations amongst the measured ratios in a chain of four or five analyses. Ap003 containing 0.45 wt.% Cl (McCubbin et al., 2012) and of $\delta^{37}Cl$ +0.3 ‰ (e.g., Williams et al., 2016) was used as the primary reference standard on 29th February 2016 when only Kalahari 009 thin section #2 was analyzed (Table 1). Ap003 gave an IMF of +16 ± 0.4 ‰ (n = 3). The reproducibility of Ap003 standard was ~0.5 ‰ over three analyses.

Additional analyses of Ap004, as well as Ap005 (0.95 wt.% Cl) and/or Ap018 (0.13 wt.% Cl) were made during each analytical day. These analyses allowed external assessment of the IMF which was within error of the primary standard and of the external precision which on Ap005 was ~1 ‰. Since the secondary standards Ap005 and Ap018 do not have reported bulk $\delta^{37}Cl$ values they were referenced to the ratio measured on the primary standard for a given day. The reproducibility of $^{37}Cl/^{35}Cl$ ratio of secondary apatite standards is shown in Figure 2 and was typically better than 2 ‰ at the 2σ level, where the uncertainties represent the combined reproducibility of the $^{37}Cl/^{35}Cl$ ratio on the primary standard and the analytical error associated with each measurement. The average $\delta^{37}Cl$ values for secondary standards obtained during the entire session were +0.6 ± 2.0 ‰ (Ap004, n = 34), +0.4 ± 2.4 ‰ (Ap005, n = 34) and +0.6 ± 2.0 ‰ (Ap018, n = 24), where the uncertainties represent the 2 standard deviations amongst the measured $^{37}Cl/^{35}Cl$ ratios referenced to Ap004 (or Ap003 in the case of the last analytical day). Ap005 and Ap018 do not yet have published bulk $\delta^{37}Cl$ values but are within error of the value for Ap004 and Ap003 that have been previously reported (as discussed above).

2.4. Protocol for measuring D/H ratio and H_2O content of apatite

In addition to obtaining Cl isotope and abundance data, D/H and H_2O data were collected by NanoSIMS for eight apatite crystals in samples 15016 and 15065 following the methods of Barnes et al. (2014). A Cs+ primary beam of ~220 pA current was used and negative secondary ions of ^{1}H, D, ^{13}C, and ^{18}O were collected simultaneously in electron multipliers. Electronic gating was used to restrict counting secondary ions from the inner 25 % of the sputtered area. Before analysis, pre-sputtering was performed over an area ~400 μm^2 using a primary beam of ~480 pA for 1 minute to clean the sample surface. An electron gun was used to provide charge compensation. Due to the variation of apatite grain size within and between samples, and the need to avoid cracks or inclusions, the analysis areas varied from 4 µm × 4 µm to 8 µm × 8 µm. Real time isotope imaging was carried out during the pre-sputtering to monitor ^{1}H and ^{13}C to identify cracks and hotspots. Occasionally, during an analysis a crack or hotspot appeared; in such a case, only the signal corresponding to analysis of the pristine sample was considered (Tartèse et al., 2013). This signal was isolated using the NanoSIMS DataEditor software developed by Frank Gyngard (Washington University). Data inclusion was based on the ^{13}C signal, which is very low in lunar apatites but is several orders of magnitude higher for material filling the cracks. The D/H ratios are henceforth expressed as δD relative to SMOW. To correct the measured D/H ratios of lunar apatites for the IMF a reference apatite was used, Ap004 (δD = -45 ± 5 ‰, McCubbin et al., 2012). The IMF (defined as $[(D/H_{measured}/D/H_{true}-1) \times 1000]$) was +285 ± 22 ‰ (n = 8). The typical reproducibility of D/H ratio on Ap004 was 24 ‰ where the uncertainty represents the 2 standard deviations amongst the measured ratios in a chain of four analyses.

For the calibration of H_2O contents, three terrestrial apatite standards Ap003 (0.06 wt.% H_2O), Ap004 (0.55 wt.% H_2O), and Ap018 (0.2 wt.% H_2O) described in McCubbin et al., (2012) pressed in indium were used (Figure A.3) along with a nominally dry San Carlos olivine crystal (blank). This 'dry' olivine was used to monitor instrumental H background expressed here as H_2O equivalent, which was ~14 ppm (Electronic Annex). A single analysis was performed on a clinopyroxene crystal in 15065, which gave ~20 ppm H_2O. Therefore, the calculated background H_2O contents for indium-pressed 'dry' olivine and epoxy-mounted nominally anhydrous clinopyroxene are similar. For further details about the contribution of background to lunar apatite analyses and correction of data for the effects of spallation at the lunar surface, the reader is referred to the Electronic Annex.

3. Sample descriptions

We investigated two Apollo 12 basalts consisting of a porphyritic pigeonite basalt (12039) and a sub-ophitic ilmenite basalt (12064). They have crystallization ages of between ~3.1 and 3.2 Ga (Meyer, 2009; Snape et al., 2016). Of the Apollo 15 basalts studied, one

sample is a vesicular, olivine-normative basalt (15016), one is a sub-ophitic, porphyritic, pigeonite basalt (15058), and one sample is a coarse-grained (pyroxene and plagioclase crystals between 2 mm and 5 mm) pigeonite basalt (15065). The Apollo 15 samples have crystallization ages ranging between ~3.3 and ~3.4 Ga (Meyer, 2009 and references therein). We investigated a single Apollo 17 sample, which is a medium-grained (crystals up to 2 mm in length), vesicular, 'unclassified' high-Ti basalt (70017) that has a crystallization age of ~3.7 Ga (Meyer, 2009 and references therein). In addition to Apollo samples, we investigated two lunar meteorites (MIL 05035 and Kalahari 009). Miller Range (MIL) 05035 is an incompatible trace element (ITE) depleted lunar gabbroic meteorite of very-low- to low-Ti bulk composition that has a crystallization age between ~3.8 and 3.9 Ga (Nyquist et al., 2007). Kalahari 009 is a fragmental basaltic meteorite containing very-low-Ti lunar basalt components (Terada et al., 2007; Sokol et al., 2008). Kalahari 009 is one of the oldest lunar basalts available for study with a crystallization age of ~4.3 Ga (Terada et al., 2007; Shih et al., 2008), and more recently defined as 4.369 ± 0.007 Ga by Snape et al. (2018). Kalahari 009 is also one of the most ITE depleted basalts, and it is suspected to have originated from the lunar farside (e.g., Shih et al., 2008; Sokol et al., 2008).

4. Mineralogical and textural occurrence of apatite in lunar basalts

Apatites were present in all eight samples, and were located in each thin section by scanning electron microscopy (SEM) following the methods detailed in Barnes et al. (2014). Figure 3 shows backscattered electron (BSE) images of some of the apatites analyzed in this study as well as details regarding their petrographic and textural context within the host sample. The Electronic Annex contains a BSE image of each of the thirty-one apatite crystals analyzed in this study (Figure A.6 to A.9).

Apatites analyzed in 12039 occur as euhedral basal and acicular to subhedral crystals, ranging from <15 to >150 μm in the longest dimension. A couple of the grains analyzed display chemical zoning in BSE images, and some grains contain μm-scale melt inclusions. Apatites in this sample occur predominantly in mesostasis regions along with troilite, residual K-rich glass, clinopyroxene, breakdown products of pyroxferroite (i.e., symplectite assemblages consisting of hedenbergite, fayalite, and silica), anorthite, potassium feldspar, and silica (Figure A.6A-6D). In 12064, apatites occur in mesostasis areas comprised of pyroxene, plagioclase, residual glass, potassium feldspar, ilmenite, silica, troilite, breakdown products of pyroxferroite, and fayalite (Figure A.6E-6G). Apatite crystals in 12064 range from euhedral to subhedral, occurring as hexagonal basal sections and acicular grains, ranging in longest dimension from ~20 to ~180 μm. Some apatite crystals contain melt and mineral inclusions.

In the Apollo 15 basalt 15016, apatites occur in mesostasis regions consisting of clinopyroxene, plagioclase, residual glass, ilmenite, troilite, fayalite, silica, potassium feldspar, and Fe-Ni metal (Figure A.7A-E). Apatites can be up to ~40 µm in the longest dimension, occurring as euhedral to anhedral crystals, some as basal sections and others contain central melt inclusions. Apatites in 15058 are found together with residual glass, pyroxene, silica, anorthite, troilite, fayalite, breakdown products of pyroxferroite, K-feldspar, and ilmenite (Figure A.8A-8C), consistent with the textural context of apatites reported by McCubbin et al. (2010b). Some apatite grains show chemical zonation in BSE images (e.g., Ap#5). Apatite crystals can be up to ~50 µm in length and show a range in crystal habit from euhedral to subhedral. Some apatites in 15058 are acicular whilst others are basal and contain melt inclusions. Apatites in 15065 occur in mesostasis regions of varying mineralogy and texture (Figure A.8D-8G). Most commonly, apatite crystals occur with zoned pyroxene, plagioclase, ilmenite, silica, residual glass, fayalite, troilite, potassium feldspar, and breakdown products of pyroxferroite. The apatite crystals in 15065 analyzed in the present study vary in the longest dimension from ~30 to ~150 µm. Apatite #10 shows some chemical zoning in the BSE images (Figure A.8D). Apatites in 15065 show a variety of crystal habits from subhedral to anhedral with some apatites containing melt inclusions. In high-Ti basalt 70017, apatites occur in mesostasis pockets that are dominated by troilite, residual glass, clinopyroxene, merrillite, plagioclase, clinopyroxene, potassium-feldspar, ilmenite, and Fe-Ni metal (Figure A.9A-9B). Apatites vary from ~20 to ~80 µm in the longest dimension, and the grains exhibit crystal habits that are subhedral to anhderal.

Apatites in MIL 05035 occur in mesostasis areas comprised of fayalite, pyroxene, zirconolite, ilmenite, spinel, silica, potassium feldspar, residual glass, and Fe-Ni metal (Figure A.9C-9D). Apatite crystals range from ~10 to ~90 µm in length and are generally anhedral and heavily fractured. Apatites in Kalahari 009 are located in interstitial mesotasis regions along with fayalite, clinopyroxene, merrillite, baddeleyite, silica, and plagioclase (Figure A.9E-9G). Some apatites in Kalahari 009 are intergrown with other mesostasis phases (e.g., Figure A.9E-F). Apatites also occur with residual glass that forms a schlieren texture, like those reported by Sokol et al. (2008) for this meteorite, we analyzed one of these grains with the NanoSIMS (Figure A.9G). Apatite crystals can be up to 20 µm in the longest dimension and are usually anhedral.

5. Results

5.1. Measuring volatiles in apatite by NanoSIMS

Using the modified protocol described above, all three of the ESCs in the X-site of apatite (Cl, H_2O equivalent, and F) were analyzed by NanoSIMS (Table 1 and Table A.3).

This allowed us to (i) compare our results to previous studies that report the abundances of one or more of these volatiles in lunar apatites, (ii) compute the stoichiometry and X-site occupancy of the grains analyzed, and (iii) evaluate how accurately and precisely our protocol can measure all three volatiles simultaneously, including F.

Firstly, the H_2O contents of apatites in 15065 measured using either the D/H-H_2O protocol or the $^{37}Cl/^{35}Cl$-abundance (Cl, H_2O and F) protocol are similar, giving us confidence, at least for relatively water-rich apatites, that we can accurately measure H_2O by NanoSIMS using two different protocols (Tables 1 and 2). Secondly, the H_2O contents of lunar apatites obtained in this study are similar to what has been published previously by The Open University NanoSIMS lab for 12064, 12039, 15058, MIL 05035, and the apatite with the highest H_2O content in Kalahari 009 (Barnes et al., 2013; Tartèse et al., 2013; Tartèse et al., 2014b). Finally, the H_2O contents of lunar apatites obtained in this study are similar to what has been published previously for many of the samples that were investigated in other laboratories (Figure 5; Greenwood et al., 2011; Boyce et al., 2015).

With regards to Cl contents, we obtained values that are also consistent with what has been published for these samples (e.g., Terada et al., 2007; Joy et al., 2008; Liu et al., 2009; McCubbin et al., 2010b; McCubbin et al., 2010a; Sharp et al., 2010a; McCubbin et al., 2011; Tartèse et al., 2013; Boyce et al., 2015) (Figure 5). For example, McCubbin et al. (2011) reported Cl contents (from electron microprobe analysis) of apatites in 15058 ranging from 0.09 to 0.60 wt.% Cl and Tartèse et al. (2013) report between ~0.17 to 0.30 wt.% Cl for apatites in different section of 15058 to the one that we studied. The results of both of those studies are highly consistent with the range that we observe for apatites in basalt 15058 (Table 1 and Figure 5).

Accurate F abundances of lunar apatites acquired by SIMS have yet to be reported (McCubbin et al., 2011). We measured F during our NanoSIMS analyses and the data can be found in the Table A.3. However, we do not discuss this data further in the paper as we believe it to be inaccurate and the reader is referred to the Electronic Annex for further information. Instead of using our measured F abundances, we follow Boyce et al. (2010) and McCubbin et al. (2011) who suggested that more accurate F abundances can be obtained by assuming the X-site is fully populated at 1 structural formula unit and calculating the maximum possible F abundance by difference from the H_2O and Cl data. Such an approach results in much more consistent F abundances across samples (Table A.3), and these values will be used in the following discussion along with the measured H_2O and Cl contents (Table 1).

5.2. Volatile abundances of apatites in lunar basalts

All of the apatites analyzed in this study, apart from Ap4 from 70017, plot close to the F-apex (fluorapatite) of the apatite volatile ternary diagram (Figure 6). The Cl and H_2O data acquired for apatites from 15016, 15065, and 70017 are consistent with the range reported for apatites from Apollo 15 low-Ti basalts (McCubbin et al., 2010b; McCubbin et al., 2010a; Sharp et al., 2010a; McCubbin et al., 2011; Tartèse et al., 2013; Barnes et al., 2016) and Apollo 17 high-Ti basalts (Greenwood et al., 2011; McCubbin et al., 2011; Boyce et al., 2015; Barnes et al., 2016), respectively. One exception to the consistency is Ap4 from 70017, which exhibits a much higher Cl content than apatites in other high-Ti basalts reported in the literature (McCubbin et al., 2011; Tartèse et al., 2013; Pernet-Fisher et al., 2014; Boyce et al., 2015; Barnes et al., 2016). It is noted that of the Apollo basalts, there is a paucity of apatite volatile data (F, Cl, and H_2O) from high-Ti basalts. Overall, we find that, of the data available on the volatile chemistry of lunar apatites, the chemistry of Apollo 12 basalts (3 different basalts) varies from ~400 to 15600 ppm Cl and <10 to >6000 ppm H_2O and in Apollo 15 basalts (4 different basalts) from ~140 to 6000 ppm Cl and <10 to ~3600 ppm H_2O. Based on the current data, the apatites in Apollo 15 basalts appear to contain less H_2O than those found in Apollo 12 basalts or low-Ti basaltic meteorite MIL 05035. Furthermore, the Apollo 12 basalts are characterized by apatites with more heterogeneous volatile contents than apatites within Apollo 15 basalts.

5.3. Evaluation of the protocol to measure Cl isotopes in apatites

Two of the samples that we studied have been independently analyzed in other laboratories. Boyce et al. (2015) analyzed apatites in a different thin section of basalt 12039 using a Cameca 7f-GEO SIMS at Caltech. They reported $\delta^{37}Cl$ values of between +16 ± 3 and +18 ± 3 ‰ (2σ). Their values are similar to the data that we obtained for apatites in 12039 (Table 1) as all but one of our analyses lie between ~+15 ± 3 to +19 ± 3 ‰ (2σ) (Figure 4). Apatites in MIL 05035 were analyzed by Wang et al. (2012) using the Caltech NanoSIMS 50L and our data (Table 1) are indistinguishable from their results. Boyce et al. (2015) also analyzed an apatite crystal in MIL 05035 reporting its Cl isotope composition as -4 ± 2 ‰. The single isotopic value of Boyce et al. (2015) is extremely light compared to the numerous results that we obtained and those of Wang et al. (2012). However, that single enigmatic discrepancy aside, the overall comparison between the data obtained from different laboratories, using different analytical procedures, on different instruments, and using different thin sections demonstrates the inter-laboratory consistency and reproducibility of performing Cl isotope measurements on lunar apatite.

5.4. Chlorine isotopic composition of apatites in lunar basalts

Forty-one measurements were made among thirty-one apatite crystals from the eight samples investigated (Table 1). In the Apollo 12 low-Ti basalts, 12039 and 12064, the $\delta^{37}Cl$ value varied from +13.6 ± 3.0 ‰ to +19.4 ± 2.6 ‰ (2σ represent combined reproducibility on standards and analytical error) and from +10.3 ± 3.0 to +14.9 ± 1.5 ‰, respectively, and the Cl content from 0.05 to 0.26 and 0.04 to 0.23 wt.%, respectively. The Apollo 15 low-Ti basalts yielded apatites with $\delta^{37}Cl$ values ranging from +9.9 ± 5.1 to +14.0 ± 2.6‰ for 15016, +7.4 ± 1.6 to +12.2 ± 1.4 ‰ for 15058, and +9.2 ± 1.1 to +12.0 ± 1.1 ‰ for apatites in 15065. The Cl content of apatites in 15016 ranged from <0.02 to 0.3 wt.%, in 15058 from 0.18 to 0.52 wt.% Cl, and in 15065 apatites contained between 0.12 and 0.44 wt.% Cl. Apollo 17 high-Ti basalt 70017 contained apatites with Cl isotopic compositions from +9.1 ± 0.6 to +19.4 ± 2.4 ‰ and Cl abundances from 0.07 to 1.47 wt.%. Lunar basaltic meteorites, MIL 05035 and Kalahari 009, yielded apatites with $\delta^{37}Cl$ values from +3.6 ± 1.3 to +7.5 ± 1.4 ‰ and +15.4 ± 1.4 to +22.4 ± 2.5 ‰, respectively. The chlorine content of apatites in MIL 05035 ranged from 0.66 to 0.95 wt.% and in Kalahari 009 from 0.08 to 0.50 wt.% Cl. There are no apparent correlations, outside of analytical uncertainty, between $\delta^{37}Cl$ and Cl content of apatites within individual samples in the present study (Figure 4).

Overall, the Apollo 15 basalts contain apatites characterized by lighter Cl isotopic compositions than the Apollo 12 basalts. For the previously unstudied samples, apatites in 12064 shows similarity to both Apollo 12 and 15 apatites in terms of both Cl isotopic composition and Cl content. Apatites in olivine basalt 15016 have Cl isotopic compositions within error of those in 12064 and olivine basalt 15555 (Sharp et al., 2010a; Barnes et al., 2016). Pigeonite basalt 15058 contains some apatites with overlapping Cl isotopic compositions to those of the other Apollo 15 basalts (Figure 4). In addition, some of the heaviest Cl isotopic values from apatites in 15058 are within error of the lightest value recorded by apatites in Apollo 12 pigeonite basalt 12039 and ilmenite basalt 12064. The Cl isotopic compositions of apatites in high-Ti 70017 are similar to the heaviest values exhibited by the other Apollo 17 high-Ti basalts (70035 and 75055) (Figure 8). Apatites in Kalahari 009 display a bi-modal distribution in both $\delta^{37}Cl$ values and Cl content outside of analytical uncertainty. Two analyses of an apatite crystal in one thin section of Kalahari 009 gave +22 ± 3 ‰ (Cl content ~800 ppm) whereas another grain in the same thin section and a third grain in a different thin section gave +15 ± 1 ‰ (Cl content 4500 to 5000 ppm). The results from Kalahari 009 are similar to the heaviest values recorded by apatites in 70017 and 12039 (Figure 4). In fact, the $\delta^{37}Cl$ values are so fractionated that they also overlap with the Cl isotopic composition of apatites in very-high K basalt 14304 (Barnes et al., 2016).

5.5. H-isotope and H_2O systematics of apatites in 15016 and 15065

New D/H-H_2O data for lunar apatites in 15016 and 15065 are reported in Table 2. The data were corrected for instrumental contributions of H and for the effects of spallation reactions that occurred at the lunar surface (details are provided in the Electronic Annex). While there are two production rates for deuterium (Merlivat et al., 1976; Füri et al., 2017), it is unclear how applicable the production rate of deuterium from Füri et al. (2017) is to cosmic-ray spallation of phosphates, so only the cosmic-ray spallation corrected δD values using the production rate of Merlivat et al. (1976) are considered here. The results for apatites in 15016 range from ~-80 to +490 ‰, and H_2O contents range from ~55 to 380 ppm. There is no clear correlation between δD and 1/H_2O systematics within the data for 15016, and there is no correlation between δD-H_2O and petrographic setting. Apatites in 15065 have δD values from ~+930 to +1080 ‰ with H_2O contents ranging from ~1820 to 2900 ppm, with no observable correlation between D/H and H_2O.

6. Discussion

6.1. Degassing and alteration

As magmas ascended and erupted onto the lunar surface they underwent degassing of volatiles, evidence of which has been demonstrated in lunar systems experimentally (Ustunisik et al., 2011; Ustunisik et al., 2015) and empirically by preserved core-rim zoning of volatiles within pyroclastic glass beads (e.g., Saal et al., 2008; Wetzel et al., 2015) and through the observation of mineralized, vapor-deposited coatings on pyroclastic glass beads (e.g., Mckay et al., 1973a; Mckay et al., 1973b). Evidence for loss of volatiles from lunar basalts also comes from vesicles in samples like 15555 and 15016, with the latter comprising ~50% vesicles by volume (Meyer, 2009), demonstrating that lunar lavas exsolved vapor phases. Various studies of lunar volatiles have speculated that the composition of those vapors could have consisted of CO (e.g., Sato, 1979; Fogel and Rutherford, 1995; Rutherford and Papale, 2009; Wetzel et al., 2013; Wetzel et al., 2015), halogen compounds (HF, HCl) (e.g., (Goldberg et al., 1976; Elkins-Tanton et al., 2003; Ustunisik et al., 2011; Ustunisik et al., 2015), S compounds (e.g., H_2S) (Ustunisik et al., 2011; Bell et al., 2015; Ustunisik et al., 2015), and/or H_2 and H_2O (e.g., Sharp et al., 2013; Tartèse et al., 2013).

The basalt suite studied here includes samples that span H-isotopic compositions from relatively unfractionated to highly fractionated values (Figure 7). Apatites in 15065 have D/H ratios that are similar to some Apollo 12 basalts (e.g., 12039 and 12064) and high-Ti basalts (e.g., 10044; Greenwood et al., 2011; Barnes et al., 2013; Boyce et al., 2015). The high δD

values (>+500 ‰) recorded by lunar basalts have been interpreted by some as the result of degassing of H_2 from their parent magmas (e.g., Saal et al., 2013; Tartèse et al., 2013; Tartèse and Anand, 2013; Tartèse et al., 2014b). If volatile degassing was a major process, then such degassing could have fractionated the H and D isotopes of H_2O in basalt 15065 to produce the high H-isotopic compositions recorded in apatite (Table 2). Conversely, low D/H ratios recorded by apatites in lunar basalts have been interpreted as (i) unfractionated and hence un-degassed, potentially original, D/H ratios (e.g., Tartèse et al., 2014b), which are similar to terrestrial mantle values and bulk carbonaceous chondrites (e.g., Alexander et al., 2012; Hallis et al., 2015), (ii) minimally degassed signatures (Tartèse et al., 2014b), (iii) mixing of a heavy, degassed value with solar-derived H from the lunar regolith following the model of Treiman et al. (2016), or (iv) in the case of meteorites, possible cryptic Antarctic water alteration (Tartèse et al., 2013). For KREEP basalt 15386, Tartèse et al. (2014b) were able to combine measurements of D/H-H_2O and the textural context of apatites to demonstrate that the data were conducive to loss of H_2 from a basaltic melt of a pre-degassing terrestrial-like D/H ratio. Treiman et al. (2016) reported that a few samples with low D/H ratios measured in relatively H_2O-poor apatites, like those from 12040, could be reconciled with assimilation of hydrogen from the hot regolith that lay beneath the 12040 lava flow. They established this by correlating the average D/H ratio and H_2O contents of apatite with the equilibration of Fe and Mg in either pyroxene or olivine (represented by the ratio of maximum Mg# of pyroxene/minimum Mg# of pyroxene or olivine) in their sample set (Treiman et al., 2016). The results for apatites in vesicular olivine basalt 15016 are comparable to that of olivine normative basalt 12040 (Greenwood et al., 2011; Boyce et al., 2015) and KREEP basalts 15386 and 72275 (Tartèse et al., 2014b) as shown in Figure 7, which are also amongst the most H_2O-poor apatites reported from lunar basalts. The variability in H-isotopic compositions of apatites in 15016 cannot be related easily to textural context, unlike apatite in 15386 (Tartèse et al., 2014b). The chemical equilibration factor for pyroxene in 15016 of 0.4 (Bence and Papike, 1972) places it within error of low-Ti basalt 12040 (Treiman et al., 2016), indicating that the thermal homogenization of Fe and Mg in pyroxene in 15016 may have coincided with a process that brought in hydrogen of a lower D/H ratio. Therefore, whilst there is no apparent textural context observed for the H isotope systematics in 15016 (nor in 15555, Tartèse et al., 2013) the fractionation of H isotopes during vapor loss cannot be ruled out nor can incorporation of assimilated H from the regolith (Treiman et al., 2016).

For some of the basalts investigated, we found significant (outside of analytical error) intra-sample variation in $\delta^{37}Cl$ values. It is possible that such intra-sample variations in Cl isotope compositions could be related to magmatic degassing of Cl. Sharp et al. (2010)

proposed that positively correlated Cl contents and Cl isotopes in apatites from several basalts could be explained by fractionation of Cl isotopes during Cl loss (as metal chlorides) from anhydrous basaltic magmas of initially similar Cl contents. We did not observe any such correlations in our apatite dataset. The largest intra-sample variations are observed for 70017 and Kalahari 009. A variation of ~5 ‰ (δ^{37}Cl) is observed between three grains in one mesostasis pocket of 70017 (Figure A.9). In Kalahari 009, the bimodal distribution in δ^{37}Cl-Cl contents cannot be related to texture. Such intra-sample variations could be related to fractionation of isotopes during basalt crystallization, however, we cannot definitively conclude this as we do not know the growth history of the apatites, and we lack textural evidence and trace element data for these grains. Whilst we do not have the textural evidence to pin point the cause of intra-sample variation in Cl isotopes, it is likely that H_2 loss was the dominant mechanism for H loss from the majority of lunar basalts studied here, and may have been concurrent with loss of other H- and halogen-bearing species including minor amounts of metal chlorides (Ustunisik et al., 2011; Ustunisik et al., 2015). In fact, it would take up to 30 % loss of Cl as metal chlorides (NaCl, $ZnCl_2$, or $FeCl_2$) from the undegassed melts to produce the intra-sample variations in δ^{37}Cl observed in 15058, 15065, and MIL 05035. Notably, the loss of HCl vapor does not cause significant fractionation of Cl isotopes (Sharp et al., 2010b).

The δ^{37}Cl and δD data for lunar basalts reveal a broad negative correlation (Figure 7). If the type of basalt is considered (i.e., KREEP, low- and high-Ti) then the data cluster into two groups: one dominated by the KREEP-rich basalts and basaltic lunar meteorites (Northwest Africa (NWA) 4472 and NWA 2977) that are characterized by relatively low δD values (and incidentally lower water contents) and high δ^{37}Cl values, and the other group is dominated by low- and high-Ti basalts having less to moderately fractionated δ^{37}Cl values and high δD values. As discussed above, the magmatic origin of the H in relatively dry samples like 15016 and 12040 are debated as they could have some regolith H component. When compared to other lunar basalts, MIL 05035 seems to be anomalous in its δD-δ^{37}Cl systematics. Antarctic weathering was ruled out by Tartèse et al. (2013) as the cause of the lower H-isotopic composition of MIL 05035 compared to other low-Ti basalts. The coupled intermediate δD values and relatively low δ^{37}Cl values also argue against significant Antarctic alteration. The volatile systematics of MIL 05035 are thus best described by having experienced less degassing than other low-Ti basalts (Tartèse et al., 2013), and this sample seems to have retained a magmatic Cl isotope composition being fractionated from 0 ‰. In both Cl and H isotopes, Kalahari 009 overlaps with H_2O-poor low-Ti basalts and KREEP-rich basalts (Figure 7), despite Kalahari 009 containing relatively H_2O-rich apatites and being more depleted in trace elements (i.e., not KREEPy).

6.2. Mixing of incompatible trace elements between mantle cumulates and urKREEP

The relationship between incompatible trace element (ITE) ratios and Cl isotopes of apatites in lunar basalts has been used as evidence for the presence of two Cl reservoirs in the lunar interior. The trend is almost exclusively based on data from Apollo samples (Boyce et al., 2015; Barnes et al., 2016). The Apollo low-Ti basalts studied exhibit a range of ITE contents (Figure 8a-c), and that when ITE contents are compared to δ^{37}Cl values, the Apollo 12 and 15 low-Ti basalts mostly overlap. Overall, the high-Ti basalts show much more variability in measured Cl isotope ratios and trace elements and scatter around the trend formed by the low-Ti basalts.

The data collected in this study fit with previous observations that the low-Ti mare basalts from Apollo 12 and 15 missions share similarities in their overall abundances of major oxides, rare earth elements, and ITEs (Figure 8a-c), suggesting that these rocks were formed from compositionally similar magmas (e.g., Kushiro and Haramura, 1971; Neal and Taylor, 1992; Schnare et al., 2008). However, differences in compatible element chemistries and in neodymium isotopic data, both within the Apollo 12 (ilmenite, olivine and pigeonite) basalts and between Apollo 12 and 15 basalts, indicate that they were derived from separate source regions within the lunar mantle (e.g., Neal and Taylor, 1992; Snyder et al., 2000; Hallis et al., 2014). Crucially, the results for the low-Ti mare basalts fall on a crude mixing trend between a hypothetical mantle Cl reservoir (~0 ‰) and urKREEP (> +25 ‰) (the latter denoted by KREEPy basalts in Figure 8; Boyce et al., 2015; Barnes et al., 2016). The Apollo 12 and 15 basalts share similar volatile element chemistries and Cl isotope compositions suggesting that although the basalts within and between these groups were derived from different sources, perhaps their ITE abundances (inclusive of volatiles) were derived from a similar reservoir, which according to prevailing models would be urKREEP (Boyce et al., 2015; Barnes et al., 2016).

For the high-Ti basalts, three basalt types (A, B, and U) are represented in the available data set and these are expected to have formed from distinct parental melts (Hallis et al., 2014). Existing petrologic models for the formation of the high-Ti mare basalts favor source region heterogeneity over assimilation (of KREEP) to explain the geochemical variations within the high-Ti group (Neal and Taylor, 1992; Hallis et al., 2014). Yet the currently available data don't show any resolvable difference between high- and low-Ti basalts, let alone within the high-Ti basalt group. Although we note that the dataset does not span the entire compositional space of the high-Ti basalts (e.g., missing high-K basalts). We suspect that other magmatic processes and or geochemical reservoirs of Cl may need to be considered when interpreting the δ^{37}Cl of the high-Ti mare basalts, though more in-depth

studies are needed to fully investigate this suite of basalts. Overall, the data presented here for Apollo basalts demonstrates clear heterogeneity in ITEs in the lunar mantle sources as sampled by the various compositional types of basalts (e.g., Fig. 9c). The data presented for these samples is consistent with mixing between mantle and urKREEP reservoirs with distinct $\delta^{37}Cl$ compositions.

6.3 Volatile reservoirs sampled by basaltic lunar meteorites

According to the classification schemes of Neal and Taylor (1992), lunar basaltic meteorite MIL 05035 has a bulk TiO_2 composition that ranges from very-low-Ti to low-Ti (Joy et al., 2008; Liu et al., 2009). Here we refer to MIL 05035 as a low-Ti basalt. MIL 05035 is a relatively evolved lunar basalt (bulk-rock Mg# 38-40; Joy et al., 2008; Liu et al., 2009). The Cl isotopic composition of apatites in MIL 05035 is similar to that of 10058 and is within error of 10044 (Figure 4). When compared to other lunar basalts, MIL 05035 has relatively low bulk-rock Th and K contents (~0.3 ppm and 120 to 360 ppm, respectively; Joy et al., 2008; Liu et al., 2009) and low $\delta^{37}Cl$ values (Figure 8). The ITE-poor nature of MIL 05035 and its pairings indicates that the parental melt was derived from an urKREEP-poor mantle source, and that the partial melt did not assimilate a significant KREEP or KREEP-like component as it ascended through the lunar mantle and crust (Joy et al., 2008). The relatively low Cl isotope composition of MIL 05035 apatites suggests that the fractionation of the parental melt to form this chemically evolved basalt had little effect in fractionating the isotopes of Cl. Calzada-Diaz et al. (2015) suggested that the YAMM group of meteorites, to which MIL 05035 is a member, most likely originated from Mare Fecunditatis. Therefore, MIL 05035 appears to describe the uncontaminated Cl isotopic composition of the lunar mantle and pins the current models for two-component mixing of Cl in the hybridized lunar interior (Boyce et al., 2015; Barnes et al., 2016; Boyce et al., 2018).

Further supporting evidence for the low-Ti mixing trend comes from the Cl isotope systematics of apatites in meteorites NWA 4472 and NWA 2977. Northwest Africa 4472 contains sub-ophitic KREEP clasts (Joy et al., 2011) containing phosphates, in which one apatite was analyzed for Cl isotopes by Tartèse et al. (2014a). These authors measured consistent $\delta^{37}Cl$ values across the clast, with an average of ~+19 ± 1 ‰ (error represents one standard deviation of reported values) (Tartèse et al., 2014a). The bulk-clast composition of this lithology is not well constrained, but Joy et al. (2011) did report the bulk K_2O content of the clast. The $\delta^{37}Cl_{ap}$ and bulk-rock K systematics fit well the mixing trend exhibited by other low-Ti basalts (Figure 8b). In addition, olivine cumulate (OC) lunar meteorite NWA 2977 (paired with NWA 773) is a VLT, KREEPy lithology (Fagan et al., 2003; Zhang et al., 2011). Wang et al. (2012) reported an average $\delta^{37}Cl$ composition of ~+20 ± 6

‰ (error represents one standard deviation of reported values) for apatites in the meteorite. Northwest Africa 2977 also falls on the mixing of ITEs between mantle cumulate and urKREEP sources (Figure 8). Joy et al. (2011) and later Calzada-Diaz et al. (2015) used Lunar Prospector Gamma-Ray FeO, TiO_2, and Th data to propose that the NWA 4472 regolith breccia originated from the Procellarum KREEP Terrane (PKT) region of the nearside, probably from areas adjacent to the Imbrium basin. Using the same approach, brecciated mafic meteorite NWA 773 was proposed to originate from either the western limb of the PKT or from deposits in Mare Serenitatis, Mare Crisium, or Mare Fecunditatis regions (Calzada-Diaz et al., 2015). The meteorites NWA 4472 and NWA 773 therefore offer additional sampling of KREEPy rocks from locations external to the areas sampled by the Apollo missions but most likely from within the PKT or from its immediate surroundings.

Barnes et al. (2016) proposed that the highly fractionated $\delta^{37}Cl$ of urKREEP was the result of impacts weakening the crust on the lunar nearside which is now recognized as the PKT. Investigating the volatile make-up of a sample derived far from the influence of the PKT (i.e., a KREEP-free sample from the lunar farside) would offer the opportunity to test this model. In contrast to the low-Ti basaltic meteorites, the age, bulk-rock chemistry (low in ITEs), and possible derivation from the lunar farside, lend promise that the Kalahari 009 meteorite could have sampled a KREEP-free lunar reservoir with a primitive volatile chemistry. The chemical composition of Kalahari 009 is unique among lunar meteorites and Apollo samples (Korotev et al., 2009). Kalahari 009 is a basalt of very-low-TiO_2 (VLT) content similar to Apollo 17 and Luna 24 basalts (Sokol et al., 2008; Korotev et al., 2009). The major oxide chemistry of Kalahari 009 (exclusive of TiO_2 content) is also similar to that of high-aluminum (HA) basalts from the Fra Mauro formation sampled by Apollo 14 (Figure A.10) and Luna 16 soils (e.g., Neal and Kramer, 2006; Shih et al., 2008). Unlike the HA basalts, Kalahari 009 is strongly depleted in rare earth elements (REEs), Ti, and especially Th, and it displays a positive Eu anomaly contrasting with most other mare basalts but being almost identical to Luna 24 basalts (Sokol et al., 2008). The Th depletion of Kalahari 009 coupled with its relatively high Cl isotopic composition cause it to fall off the trends exhibited by MIL 05035, the low-Ti basalts, and KREEP-rich basalts (Figure 8a). In $\delta^{37}Cl$-La/Sm_n space, Kalahari 009 plots in the region of the low-Ti basalts (Figure 8c). Kalahari 009 has a relatively high K_2O content, which is counter to most other lunar rocks where incompatible trace element abundances positively correlate with K_2O abundances (Boyce et al., 2018). Sokol et al. (2008) suggested that post-fall weathering of Kalahari 009 increased the bulk K_2O content of the meteorite, although the highly fractionated Cl isotopes in Kalahari 009 negate significant terrestrial alteration of volatiles in apatite (Figure 7). In summary, the

Kalahari 009 basalt is an enigmatic sample that does not fit the trends established between mare basalts, KREEP-rich basalts, and other lunar basaltic meteorites (Figure 8).

The VLT composition, depleted trace element chemistry, and positive Eu anomaly of Kalahari 009 indicate that it was derived from a mantle source that had not seen significant plagioclase extraction (Sokol et al., 2008; Korotev et al., 2009). The solubility of chloride in basaltic melts and the likely presence of a lunar atmosphere at that early stage of lunar differentiation, indicate that Cl would not have been lost from the lunar magma ocean in significant proportions until much later (Barnes et al., 2016). Therefore, we would expect the source of Kalahari 009 to have had an unfractionated Cl isotopic composition. Since the Kalahari 009 meteorite contains apatite with fractionated Cl isotopes, this indicates that the rock does not preserve a mantle-like Cl isotope signature.

Among other indicators, the ancient crystallization age (~4.35 ± 0.15 Ga, (Terada et al., 2007; Shih et al., 2008; Snape et al., 2018) and negligible HSE abundances (Sokol et al., 2008; Korotev et al., 2009) of Kalahari 009 have been used to suggest that it represents an ancient buried lava flow, a so called 'cryptomare'. The Kalahari 009 meteorite is classified as a monomict breccia of shock stage 4 and it contains potential indicators of shock melting such as schlieren (Fig. A.9) and areas of matrix cemented by impact melt (Sokol et al., 2008). Is it possible then that impacts could have reset or overprinted the volatile inventory of this meteorite? Kalahari 009 has been dated using the U-Pb system in apatite, which means that since ~4.35 Ga this rock did not experience shock temperatures above ~450-500 ˚C, temperatures above which would reset the U-Pb system in phosphate (Cherniak et al., 1991; Krogstad and Walker, 1994; Chamberlain and Bowring, 2001). This suggests that impacts, like those that brecciated the meteorite, likely did not reach the temperatures required to significantly alter the chemistry of apatite. In fact, one of the apatites we investigated is in contact with a melt schlieren (Figure A.9G), it does not have the most fractionated $\delta^{37}Cl$ value of this sample and has the same isotopic composition as a grain not co-located with impact features. Thus, it is unlikely that post-crystallization impact events significantly fractionated Cl isotopes in Kalahari 009. There is a remote possibility that the Kalahari 009 basalt could represent an impact melt formed from ancient lava flow mixed with primordial crustal material (to explain the elevated Al_2O_3 content, for example), perhaps by shockwave melting rather than direct impact melting. If that was the case then 1) the Kalahari 009 melt did not sample any of the impactor material (including volatiles), to account for the low HSE abundances (Korotev et al., 2009), 2) the ancient age would represent the cooling age of the impact melt, and 3) the impact processing fractionated the isotopes of Cl. Any impact processing of the Kalahari 009 may also have changed or

overprinted the original H content and isotopic composition of the basalt, such as addition of volatiles from the lunar regolith (Treiman et al., 2014).

In light of the chemical similarities between Kalahari 009 and the HA basalts, it is useful to explore whether they share a history involving volatiles. Potts et al. (2018) observed fractionated Cl isotope compositions in HA rocks from Apollo 14 with ages between ca. 3.9 and 4 Ga. Their sample set included both HA impact melt rocks and HA basalts with all samples displaying the same volatile systematics regardless of petrogenesis (Figure 4). The HA rocks they investigated have variable bulk ITE abundances (Figure 8) and, like Kalahari 009, their Cl isotope signatures cannot be easily related to their ITE contents (Figure 8). In order to explain their highly variable data, Potts et al. (2018) concluded that the magmatic volatile inventories of the HA basalts had been partially to fully overprinted by metasomatism involving volatile-rich vapors during the crystallization of the basalts and impact melts. This process is similar to the fumerolic activity invoked by Shearer et al. (2014) to explain the volatile signatures of 66095 and vapor metasomatism of impactite 79215 (Treiman et al., 2014). Kalahari 009 shows much less intra-sample variation in Cl isotopes than HA basalts. If Kalahari 009 was altered by Cl-rich vapors while it crystallized, and that metasomatic process was driven by impact events, then vapor metasomatism of the lunar crust could have been widespread geographically and temporally. However, to confirm whether or not metasomatism was an important process affecting this sample, we would require other trace element data.

The available data, therefore, lead us to suggest that the highly fractionated Cl isotopic compositions recorded by apatites in Kalahari 009 are not reflective of its mantle source but rather are best described as the result of volatile degassing, alteration, or secondary metasomatism, which could be related to impact processes.

6.4 Isotope fractionation during the earliest history of the Moon

Evaporative loss of Cl, as metal chlorides, from the Moon is the preferred mechanism for achieving the heavily fractionated Cl isotope values recorded in lunar samples (Sharp et al., 2010a; Boyce et al., 2015). Earlier work by Sharp et al. (2010) suggested that it was degassing of metal chlorides during basaltic eruption that fractionated the isotopes of Cl. As we have discussed, this late-stage degassing could account for the variation in Cl isotope compositions observed for apatites in some individual samples (Figure 7). However, to explain the relationships between numerous proxies for KREEP (examples K, Th, La/Sm, Figure 8) and average δ^{37}Cl values for apatites in mare and KREEP-rich basalts, a process must have occurred to create reservoirs in the Moon that have distinct Cl isotope compositions – a relatively unfractionated and Cl-poor mantle source and a highly

fractionated and Cl-rich urKREEP source (Boyce et al., 2015; Barnes et al., 2016; Boyce et al., 2018).

Previous studies have speculated upon the timing of formation of these two reservoirs to either formation during LMO crystallization (Boyce et al., 2015) or shortly after the generation of urKREEP (Barnes et al., 2016). Other isotopic evidence is emerging from moderately volatile elements that could support volatile loss during the existence of the LMO before cumulate overturn, including bulk rock S, Zn, Cl, K (Day and Moynier, 2014; Kato et al., 2015; Day et al., 2017; Dhaliwal et al., 2018) and Ga (Kato and Moynier, 2017) isotopes. Within those respective datasets, the authors observed correlations whereby the mare basalts were characterized by lighter values than the highlands/crustal samples investigated, consistent with the trends in Cl isotopes (Barnes et al., 2016). Recently, a study of the Cl isotopic composition of apatite in eucrite meteorites (Sarafian et al., 2017) showed a similar trend between Cl isotopes and bulk-rock trace elements to the one shown in Figure 8. Sarafian et al. (2017) suggested that magma ocean degassing, via loss of metal chlorides, on the eucrite parent body could explain their Cl isotope data. They also compared their data to bulk rock Zn isotope data and showed that the samples with the highest δ^{37}Cl values also had the most fractionated Zn isotopic compositions. In culmination, these independent lines of evidence support mass-dependent isotope fractionation via evaporative loss of metal chlorides as a viable loss mechanism for Cl under high temperature conditions, possibly during a magma ocean stage of planetary evolution.

Barnes et al. (2016) postulated that the evaporative loss of Cl from the LMO occurred shortly after the urKREEP reservoir had been formed and proposed that degassing was facilitated at that time by weakening of the crust through large impacts. They postulated that the PKT was evidence of such a large-scale impact event that permitted urKREEP to degas by exposing KREEPy material to the lunar surface. If the PKT is an ancient impact structure that resulted in urKREEP on the lunar nearside to have a δ^{37}Cl value of ~+30 ‰, then one would expect samples derived from outside of the PKT to deviate from the trend observed for PKT-derived basalts. Based on previous studies, Kalahari 009 should represent the best candidate for establishing the Cl isotopic composition of a KREEP-free lunar mantle reservoir because it is reported to have originated on the lunar farside - possibly Mare Marginis (Shih et al., 2008) or Mendel-Rydberg basin (Calzada-Diaz et al., 2015) - far from the influence of the PKT. However, as discussed, the highly fractionated Cl isotope compositions measured do not fit the prevailing models explaining Cl isotope fractionation on the Moon (Boyce et al., 2015; Barnes et al., 2016). In fact, the isotopic composition of Cl in the Kalahari 009 basalt is unlikely to be genetically linked to its primitive mantle source but was artificially raised by either magmatic or secondary processes. So, it seems that until

data is collected on a wider range of non-KREEPy lunar basalts and basaltic lunar meteorites, the PKT model for nearside loss of volatiles cannot be fully tested.

Conclusions

In this study, we have reported the Cl isotope compositions and volatile abundances of apatites in eight lunar samples. The data obtained on the low-Ti basalts from Apollo 12 and 15 and on lunar basaltic meteorite MIL 05035 agree well with previously reported data for low-Ti basalts. These samples fit reasonably well the mixing trends reported by Boyce et al. (2015) and Barnes et al. (2016), as δ^{37}Cl values in apatites are positively correlated with bulk trace element abundances for low-Ti basalts (inclusive of low-Ti, KREEP basalts). This trend has been interpreted as evidence that incompatible trace elements, including Cl, were concentrated in the urKREEP residual liquid of the LMO and that Cl had a highly fractionated Cl isotopic composition. The source regions for these basalts were likely created by variable mixing between the mantle (highly depleted in Cl and relatively unfractionated) and urKREEP. The high-Ti basalts scatter around the trend formed by the low-Ti basalts. Given the limited data available for the high-Ti basalts, more work is needed to firmly establish their relationship to urKREEP. We showed that the majority of lunar basalts contain Cl that records the fractionation of Cl from urKREEP on the lunar nearside, possibly related to the formation of the PKT. Kalahari 009 is a very low-Ti basalt that is extremely depleted in incompatible trace elements, and yet it contains apatites characterized by Cl isotope compositions up to 10 ‰ higher than MIL 05035. We propose that although Kalahari is an ancient lunar basalt of essentially KREEP-free composition, its Cl isotope systematics indicate it does not preserve a mantle signature. Therefore, systematic characterization of other KREEP-free lunar basaltic meteorites or clasts in polymict breccias are needed to fully test the model of Barnes et al. (2016) that calls for the early loss of volatiles from the lunar nearside PKT region of the Moon.

Acknowledgements

We would like to thank NASA's Curation and Analysis Planning Team for Extraterrestrial Materials (CAPTEM) for allocation of Apollo samples and the lunar meteorite MIL 05035 for this study. The US Antarctic meteorite samples are recovered by the Antarctic Search for Meteorites (ANSMET) program which has been funded by NSF and NASA and characterized and curated by the Department of Mineral Sciences of the Smithsonian Institution and Astromaterials Acquisition and Curation Office at NASA Johnson Space Center. Addi Bischoff is thanked for allocation of Kalahari 009 to this work. We thank Marc Norman and James Day for the editorial handling of this manuscript and for very helpful reviews. We also thank Adam Sarafian, Steve Elardo, and an anonymous reviewer for their

constructive criticisms and insightful reviews that helped to improve this manuscript. This work was supported by UK Science and Technology Facilities Council (grant # ST/L000776/1 to M.A. and I.A.F.). F.M.M. acknowledges support from NASA's Planetary Science Research Program. J.J.B. would like to thank the NASA Post-Doctoral Program for the fellowship under which the majority of the manuscript writing was completed. Romain Tartèse, Jeremy Boyce, and Rosalind Armytage are thanked for fruitful discussions.

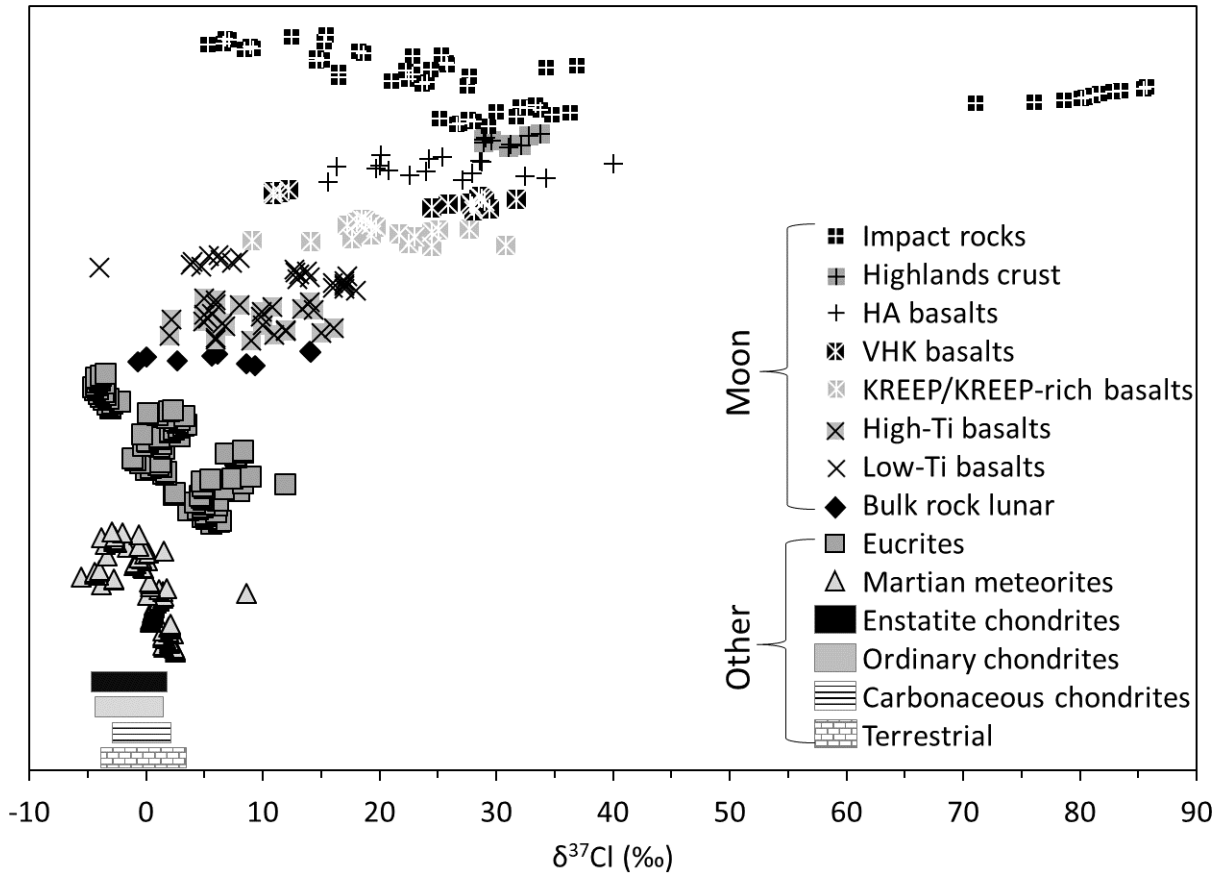

Figure 1. Chlorine isotopic composition of lunar and other Solar System materials. Lunar data sources: (Sharp et al., 2010a; Wang et al., 2012; Tartèse et al., 2014b; Treiman et al., 2014; Boyce et al., 2015; Barnes et al., 2016; Potts et al., 2018). Other data sources: (Sharp et al., 2007; Barnes et al., 2009; Sharp et al., 2013b; Sharp et al., 2016; Williams et al., 2016; Bellucci et al., 2017; Sarafian et al., 2017).

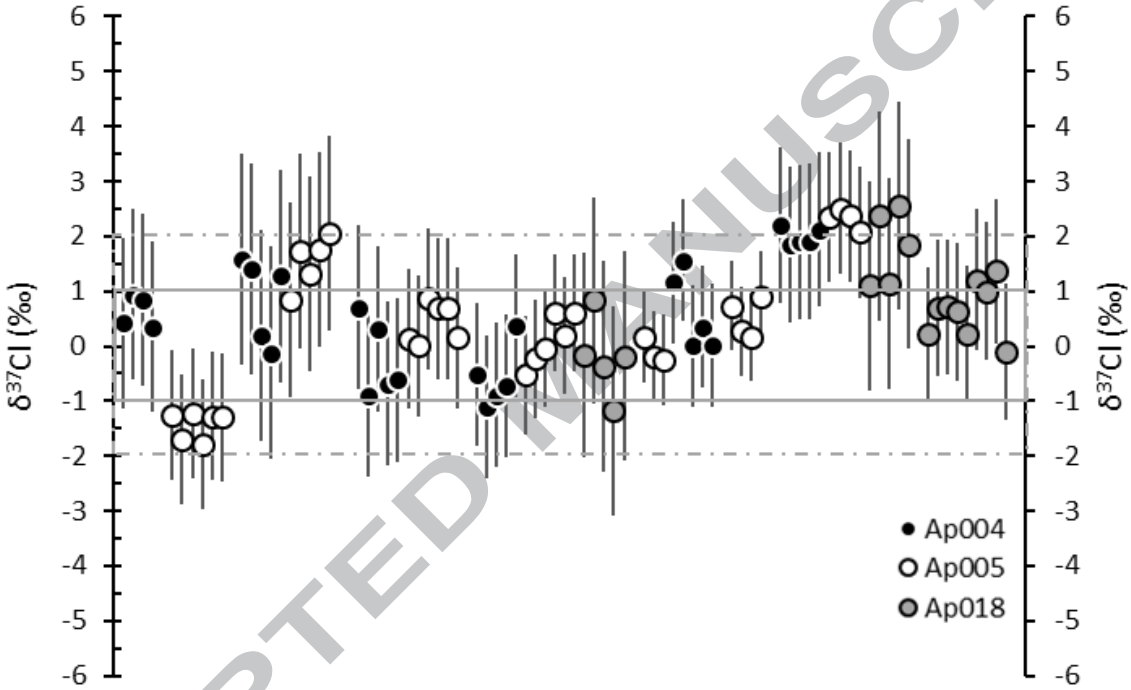

Figure 2. Plot showing the stability and reproducibility of the Cl isotopic composition measured on secondary apatite standards Ap005 and Ap018, and repeat measurements of Ap004. The data was collected over the course of a ~week analytical session. All data was referenced to the average measured $^{37}Cl/^{35}Cl$ ratio of Ap004 standard run at the beginning of each day. Error bars represent 2σ uncertainty.

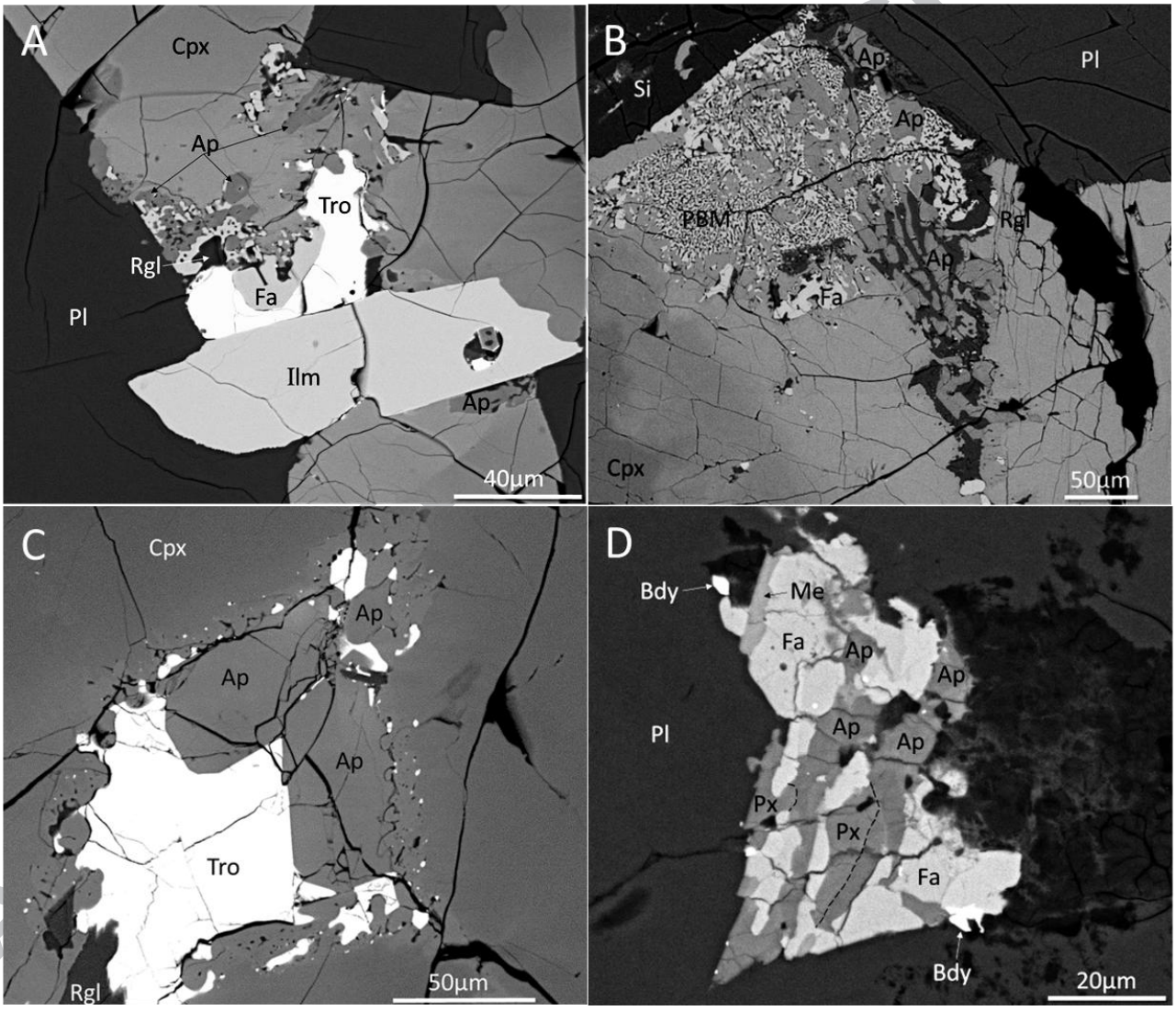

Figure 3. Backscattered electron (BSE) images of selected apatite crystals analyzed in this study from (A) 15016, (B) 15065), (C) 70017, and (D) Kalahari 009. Mineral abbreviations are as follows: Ap = apatite, Tro = troilite, PBM = pyroxferroite breakdown material, Cpx = clinopyroxene, Rgl = residual glass, Ilm = ilmenite, Pl = plagioclase, Si = silica, Me = merrillite, Bdy = baddeleyite, and Fa = fayalite. BSE images of all of the apatites analyzed in this study can be found in the Electronic Annex.

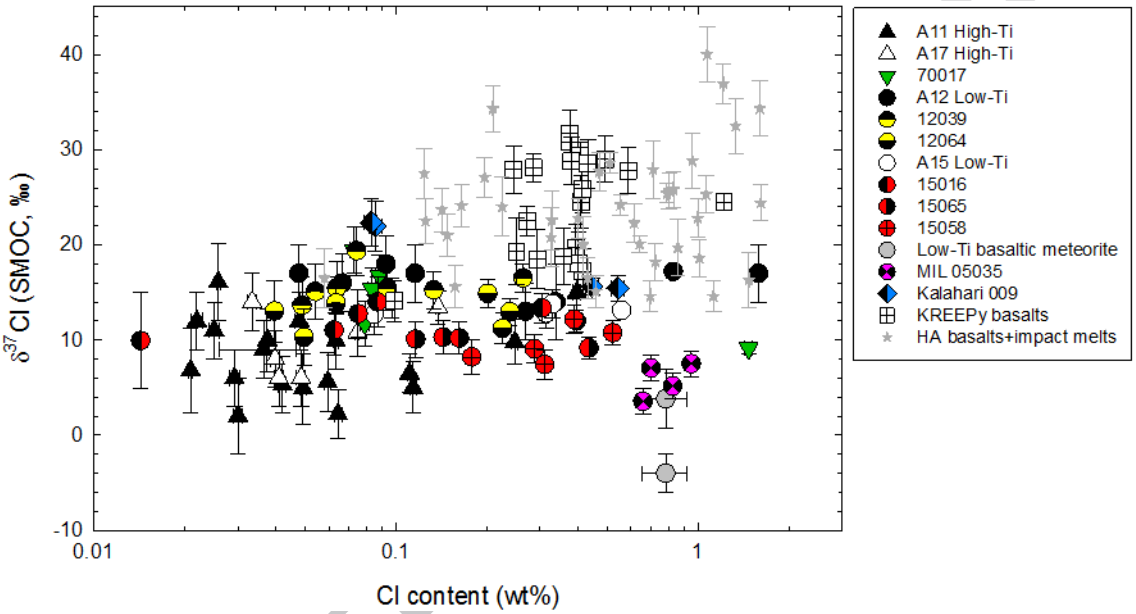

Figure 4. Chlorine isotopic composition (‰) versus Cl content (wt%) of lunar apatite analyzed in this study. Error bars represent 2σ uncertainties. Black and white symbols represent literature data: (Sharp et al., 2010a; Wang et al., 2012; Tartèse et al., 2014a for KREEP basalt clast from NWA 4472; Boyce et al., 2015; Barnes et al., 2016). The data plotted from Wang et al. (2012) uses the lowest δ^{37}Cl value reported for MIL 05035. The average Cl content of apatite in MIL 05035 obtained in this study was used to plot the isotope data from Boyce et al. (2015) and Wang et al. (2012). Data for high aluminum basalts and impact melt rocks are in grey stars (Potts et al., 2018).

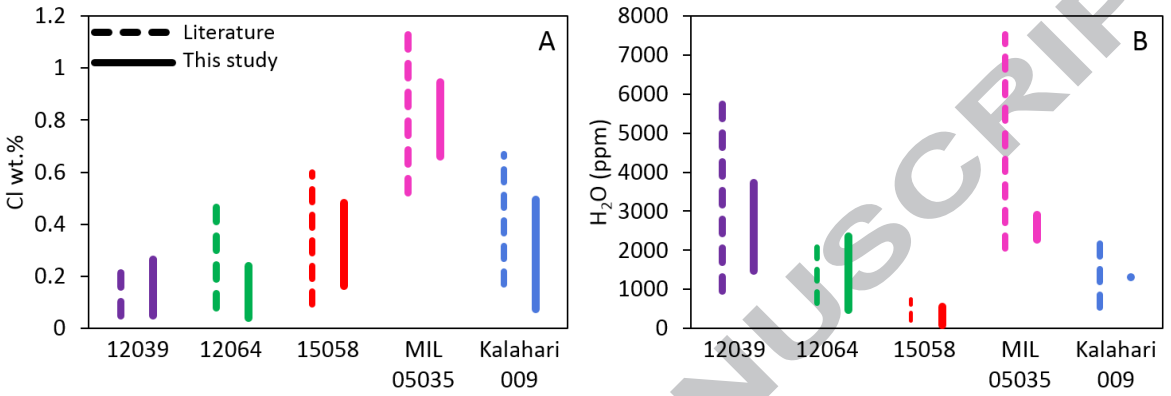

Figure 5. Plots comparing the measured (A) Cl (wt.%) and (B) H_2O (ppm) of apatite in this study (by NanoSIMS) to literature data for samples 12039, 12064, 15058, MIL 05035, and Kalahari 009. Data sources: 12039 (Cl+H_2O) (Tartèse et al., 2013), (Cl+H_2O) (Boyce et al., 2015), (H_2O) (Greenwood et al., 2011); 12064 (Cl) (Tartèse et al., 2013), (H_2O) (Barnes et al., 2013); 15058 (Cl) (McCubbin et al., 2010b; McCubbin et al., 2011), (Cl+ H_2O) (Tartèse et al., 2013); MIL 05035 (Cl) (Joy et al., 2008), (Cl) (Liu et al., 2009), (H_2O) (Tartèse et al., 2013); and Kalahari 009 (Cl) (Terada et al., 2007), (H_2O) (Tartèse et al., 2014a). Note that all of the H_2O data reported in the literature was acquired by SIMS techniques, whereas Cl was mostly measured by EPMA, except Cl data from Boyce et al. (2015) that was acquired by SIMS.

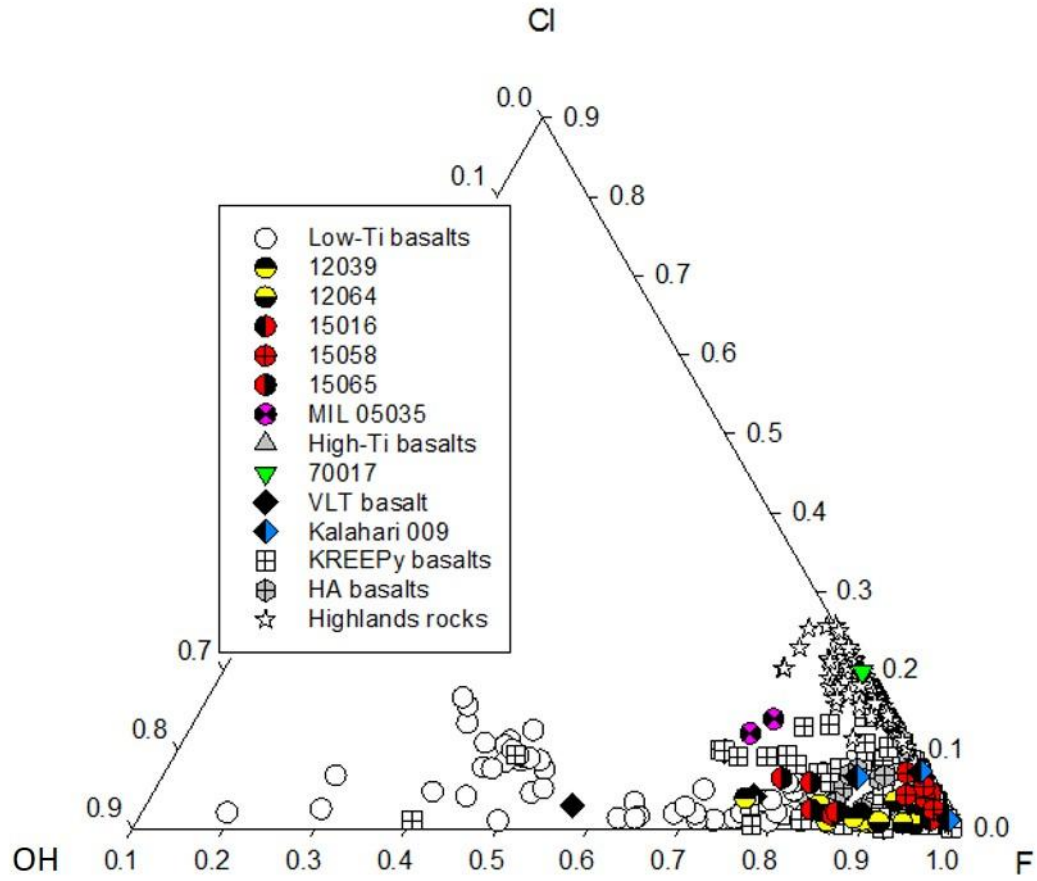

Figure 6. F, Cl, and OH chemistry of lunar apatite. The plot includes NanoSIMS data from this study and data collected by either SIMS or electron microprobe techniques from the following studies: (Fagan et al., 2003; Terada et al., 2007; Joy et al., 2008; Liu et al., 2009; Boyce et al., 2010; McCubbin et al., 2010b; Joy et al., 2011; McCubbin et al., 2011; Elardo et al., 2012; Tartèse et al., 2013; Barnes et al., 2014; Boyce et al., 2014; Elardo et al., 2014; Pernet-Fisher et al., 2014; Tartèse et al., 2014a; Tartèse et al., 2014b; McCubbin et al., 2015b; Barnes et al., 2016). For F and Cl data collected by electron microprobe the data were summed, and full X-site occupancy assumed (X = 1), the missing component was assigned to OH. All data from this study, and where necessary SIMS literature data, were normalized so that X = 1 and F was assigned as the missing component.

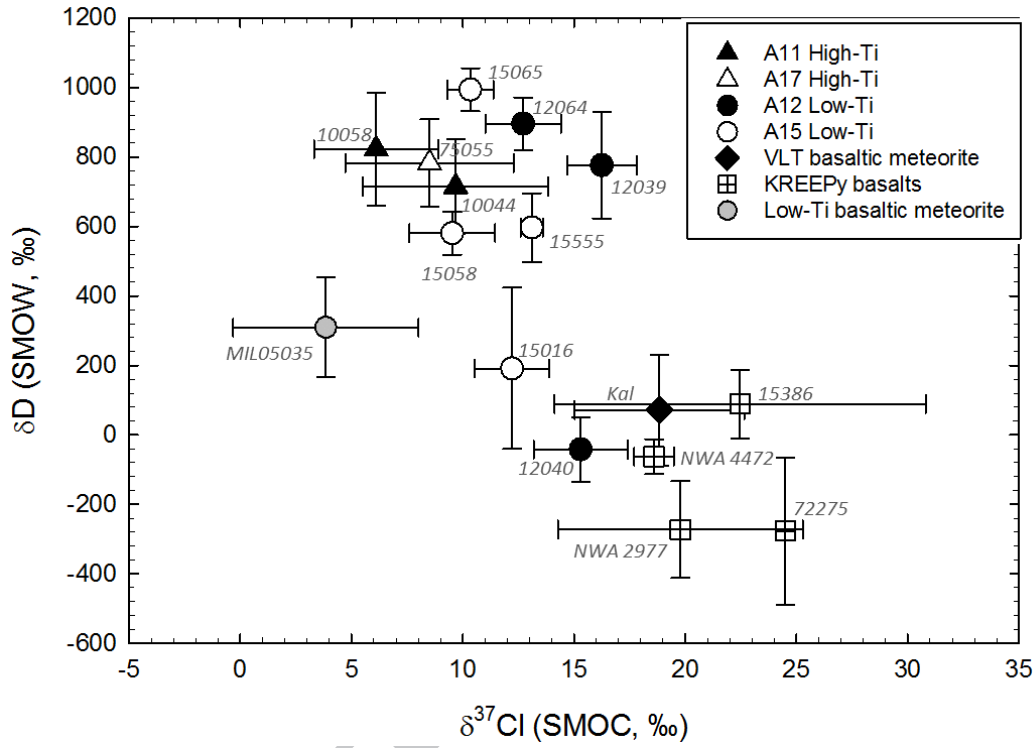

Figure 7. Average δD (‰) versus average δ^{37}Cl (‰) data for apatite in Apollo samples and lunar basaltic meteorites from the literature and this study. Error bars represent one standard deviation amongst compiled values from the following data sources: (Greenwood et al., 2011; Wang et al., 2012; Barnes et al., 2013; Tartèse et al., 2013; Tartèse et al., 2014a; Tartèse et al., 2014b; Boyce et al., 2015; Barnes et al., 2016). Data for KREEPy basalts represents the average δ^{37}Cl values for each. The H-isotope data for NWA 773 (Tartèse et al., 2014b) was plotted with the average δ^{37}Cl data for apatite in paired meteorite NWA 2977 from (Wang et al., 2012). Only the least fractionated δD values from (Tartèse et al., 2014b) were used for samples 72275, 15386, and NWA 773.

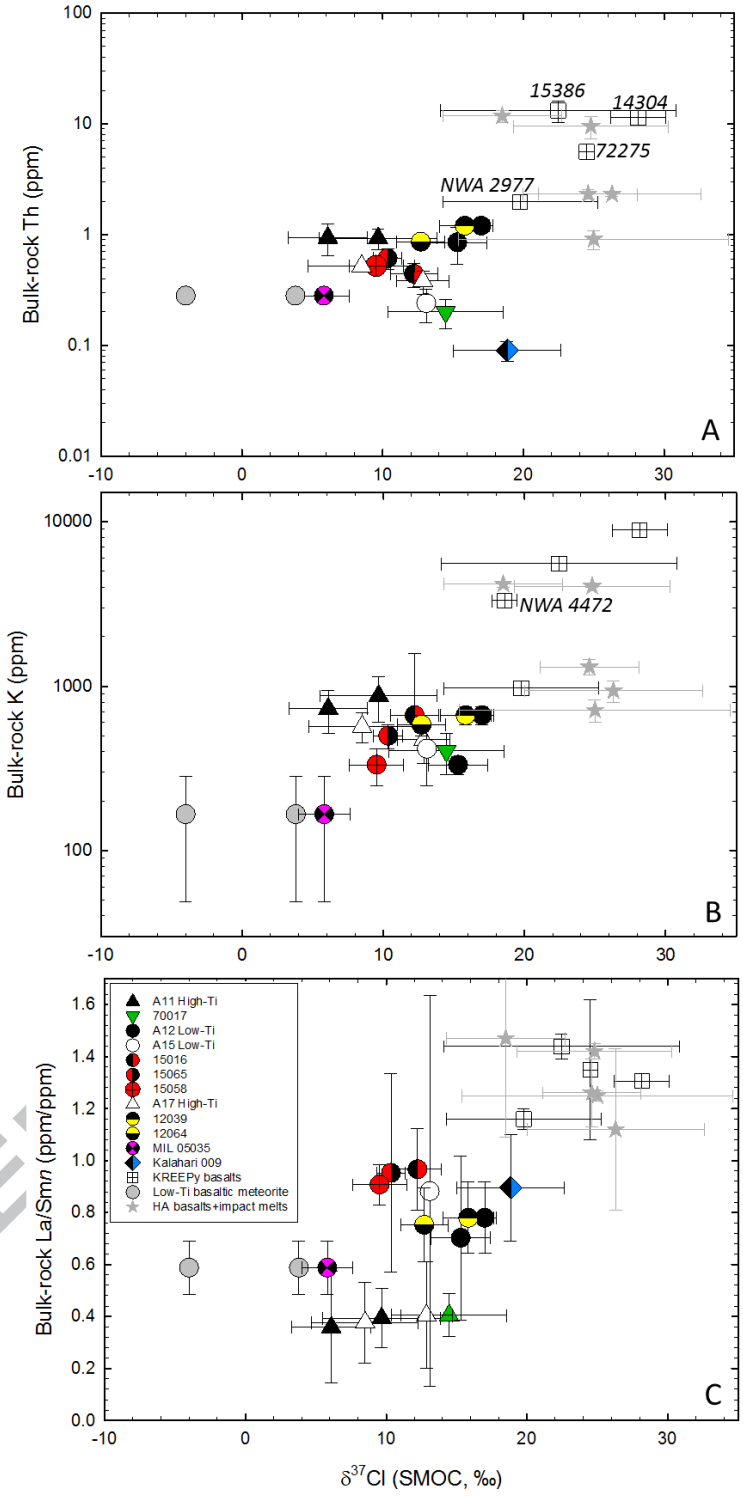

Figure 8. Plots showing the relationships between Cl isotopic composition of apatite with different bulk rock indicators of KREEP: (A) average bulk-rock Th abundance (ppm), (B) average bulk-rock K abundance (ppm), and (C) average bulk-rock CI-Chondrite normalized La/Sm ratio versus average Cl isotopic composition of apatite from lunar samples from this study and the literature. Error bars represent one standard deviation of the compiled values. Data sources for δ^{37}Cl values are same as Figure 4 caption. Data sources for basalt chemistry from Lunar Sample Compendium (Meyer, 2009) and references therein, and Fagan et al., 2003; Neal and Kramer, 2006; Joy et al., 2008; Sokol et al., 2008; Korotev et al., 2009; Liu et al., 2009; Zhang et al., 2011; Hallis et al., 2014.

References

Alexander C. M. O., Bowden R., Fogel M. L., Howard K. T., Herd C. D. K. and Nittler L. R. (2012) The Provenances of Asteroids, and Their Contributions to the Volatile Inventories of the Terrestrial Planets. *Science (80-.).* **337**, 721–723.

Barnes J. D. and Sharp Z. D. (2017) Chlorine isotope geochemistry. *Rev. Mineral. Geochemistry* **82**, 345–378.

Barnes J. D., Sharp Z. D. and Fischer T. P. (2008) Chlorine isotope variations across the Izu-Bonin-Mariana arc. *Geology* **36**, 883–886.

Barnes J. D., Sharp Z. D., Fischer T. P., Hilton D. R. and Carr M. J. (2009) Chlorine isotope variations along the Central American volcanic front and back arc. *Geochemistry, Geophys. Geosystems* **10**, 1–17.

Barnes J. J., Franchi I. A., Anand M., Tartèse R., Starkey N. A., Koike M., Sano Y. and Russell S. S. (2013) Accurate and precise measurements of the D/H ratio and hydroxyl content in lunar apatites using NanoSIMS. *Chem. Geol.* **337–338**, 48–55.

Barnes J. J., Tartèse R., Anand M., McCubbin F. M., Franchi I. A., Starkey N. A. and Russell S. S. (2014) The origin of water in the primitive Moon as revealed by the lunar highlands samples. *Earth Planet. Sci. Lett.* **390**, 244–252.

Barnes J. J., Tartèse R., Anand M., McCubbin F. M., Neal C. R. and Franchi I. A. (2016) Early degassing of lunar urKREEP by crust-breaching impact(s). *Earth Planet. Sci. Lett.* **447**, 84–94.

Bell A. S., Shearer C., deMoor J. M. and Provencio P. (2015) Using the sulfide replacement petrology in lunar breccia 67915 to construct a thermodynamic model of S-bearing fluid in the lunar crust. *Geochim. Cosmochim. Acta* **171**, 50–60. Available at: http://dx.doi.org/10.1016/j.gca.2015.08.002.

Bellucci J. J., Whitehouse M. J., John T., Nemchin A. A., Snape J. F., Bland P. A. and Benedix G. K. (2017) Halogen and Cl isotopic systematics in Martian phosphates: Implications for the Cl cycle and surface halogen reservoirs on Mars. *Earth Planet. Sci. Lett.* **458**, 192–202. Available at: http://dx.doi.org/10.1016/j.epsl.2016.10.028.

Bence A. E. and Papike J. J. (1972) Pyroxenes as recorders of lunar basalt petrogenesis: Chemical trends due to crystal-liquid interaction. *Geochim. Cosmochim. Acta* **1**, 431–469.

Boudreau A. and Simon A. (2007) Crystallization and Degassing in the Basement Sill, McMurdo Dry Valleys, Antarctica. *J. Petrol.* **48**, 1369–1387.

Boyce J. W., Kanee S. A., McCubbin F. M., Barnes J. J., Bricker H. and Treiman A. H. (2018) Early loss, fractionation, and redistribution of chlorine in the Moon as revealed by the low-Ti lunar mare basalt suite. *Earth Planet. Sci. Lett.* **500**, 205–214. Available at: https://doi.org/10.1016/j.epsl.2018.07.042.

Boyce J. W., Liu Y., Rossman G. R., Guan Y., Eiler J. M., Stolper E. M. and Taylor L. A. (2010) Lunar apatite with terrestrial volatile abundances. *Nature* **466**, 466–470.

Boyce J. W., Tomlinson S. M., McCubbin F. M., Greenwood J. P. and Treiman A. H. (2014) The Lunar Apatite Paradox. *Science (80-.).* **344**, 400–402.

Boyce J. W., Treiman A. H., Guan Y., Ma C., Eiler J. M., Gross J., Greenwood J. P. and

Stolper E. M. (2015) The chlorine isotope fingerprint of the lunar magma ocean. *Sci. Adv.* **1**. Available at: http://advances.sciencemag.org/content/1/8/e1500380/tab-pdf [Accessed June 2, 2017].

Brearley A. J. and Jones R. H. (1998) Chondritic Meteorites. In *Reviews in Mineralogy and Geochemistry* (ed. J. J. Papike). Mineralogical Society of America. pp. 3-01-3–370.

Calzada-Diaz A., Joy K. H., Crawford I. A. and Nordheim T. A. (2015) Constraining the source regions of lunar meteorites using orbital geochemical data. *Meteorit. Planet. Sci.* **50**, 214–228.

Chamberlain K. R. and Bowring S. A. (2001) Apatite–feldspar U–Pb thermochronometer: a reliable, mid-range (~450°C), diffusion-controlled system. *Chem. Geol.* **172**, 173–200.

Cherniak D. J., Lanford W. A. and Ryerson F. J. (1991) Lead diffusion in apatite and zircon using ion implantation and Rutherford Backscattering techniques. *Geochim. Cosmochim. Acta* **55**, 1663–1673.

Chu M. F., Wang K. L., Griffin W. L., Chung S. L., O'Reilly S. Y., Pearson N. J. and Lizuka Y. (2009) Apatite composition: tracing petrogenetic processes in Transhimalayan granitoids. *J. Petrol.* **50**, 1829–1855.

Day J. M. D. and Moynier F. (2014) Evaporative fractionation of volatile stable isotopes and their bearing on the origin of the Moon. *Philos. Trans. R. Soc. A* **372**, 1–26. Available at: http://dx.doi.org/10.1098/rsta.2013.0259.

Day J. M. D., Moynier F. and Shearer C. K. (2017) Late-stage magmatic outgassing from a volatile-depleted Moon. *Proc. Natl. Acad. Sci.* **114**, 9547–9551. Available at: http://www.pnas.org/lookup/doi/10.1073/pnas.1708236114.

Dhaliwal J. K., Day J. M. D. and Moynier F. (2018) Volatile element loss during planetary magma ocean phases. *Icarus* **300**, 249–260.

Elardo S. M., McCubbin F. M. and Shearer C. K. (2012) Chromite symplectites in Mg-suite troctolite 76535 as evidence for infiltration metasomatism of a lunar layered intrusion. *Geochim. Cosmochim. Acta* **87**, 154–177.

Elardo S. M., Shearer C. K., Fagan A. L., Borg L. E., Gaffney A. M., Burger P. V., Neal C. R., Fernandes V. A. and Mccubbin F. M. (2014) The origin of young mare basalts inferred from lunar meteorites Northwest Africa 4734, 032, and LaPaz Icefield 02205. *Meteorit. Planet. Sci.* **49**, 261–291.

Elkins-Tanton L. T., Chatterjee N. and Grove T. L. (2003) Magmatic processes that produced lunar fire fountains. *Geophys. Res. Lett.* **30**, 1513.

Fagan T. J., Taylor G. J., Keil K., Hicks T. L., Killgore M., Bunch T. E., Wittke J. H., Mittlefehldt D. W., Clayton R. N., Mayeda T. K., Eugster O., Lorenzetti S. and Norman M. D. (2003) Northwest Africa 773: Lunar origin and iron-enrichment trend. *Meteorit. Planet. Sci.* **38**, 529–554. Available at: http://meteoritics.org.

Fogel R. A. and Rutherford M. J. (1995) Magmatic volatiles in primitive lunar glasses: I. FTIR and EPMA analyses of Apollo 15 green and yellow glasses and revision of the volatile-assisted fire-fountain theory. *Geochim. Cosmochim. Acta* **59**, 201–215.

Füri E., Deloule E. and Trappitsch R. (2017) The production rate of cosmogenic deuterium at the Moon's surface. *Earth Planet. Sci. Lett.* **474**, 76–82. Available at: http://dx.doi.org/10.1016/j.epsl.2017.05.042.

Goldberg R. H., Tombrello T. A. and Burnett D. S. (1976) Fluorine as a consistuent in lunar magmatic gases. In *Lunar and Planetary Science Conference* pp. 1597–1613.

Greenwood J. P., Itoh S., Sakamoto N., Warren P., Taylor L. and Yurimoto H. (2011) Hydrogen isotope ratios in lunar rocks indicate delivery of cometary water to the Moon. *Nat. Geosci.* **4**, 79–82.

H. Y. McSween J. (1994) What we have learned about Mars from SNC meteorites. *Meteoritics* **29**, 757–779.

Hallis L. J., Anand M. and Strekopytov S. (2014) Trace-element modelling of mare basalt parental melts: Implications for a heterogeneous lunar mantle. *Geochim. Cosmochim. Acta* **134**, 289–316.

Hallis L. J., Huss G. R., Nagashima K., Taylor G. J., Halldorsson S. A., Hilton D. R., Mottl M. J. and Meech K. J. (2015) Evidence for primordial water in Earth's deep mantle. *Science (80-.).* **350**, 795–797. Available at: http://www.sciencemag.org/cgi/doi/10.1126/science.aac4834.

Hallis L. J., Taylor G. J., Nagashima K. and Huss G. R. (2012) Magmatic water in the martian meteorite Nakhla. *Earth Planet. Sci. Lett.* **359–360**, 84–92.

Hughes J. . and Rakovan J. . (2015) Structurally Robust, Chemically Diverse: Apatite and Apatite Supergroup Minerals. *Elements* **11**, 165–170. Available at: http://elements.geoscienceworld.org/content/gselements/11/3/165.full.pdf [Accessed June 2, 2017].

Jones R. H., McCubbin F. M., Dreeland L., Guan Y., Burger P. V. and Shearer C. K. (2014) Phosphate minerals in LL chondrites: A record of the action of fluids during metamorphism on ordinary chondrite parent bodies. *Geochim. Cosmochim. Acta* **132**, 120–140.

Jones R. H., McCubbin F. M. and Guan Y. (2016) Phosphate minerals in the H group of ordinary chondrites, and fluid activity recorded by apatite heterogeneity in the Zag H3-6 regolith breccia. *Am. Mineral.* **101**, 2452–2467.

Joy K. H., Burgess R., Hinton R., Fernandes V. A., Crawford I. A., Kearsley A. T. and Irving A. J. (2011) Petrogenesis and chronology of lunar meteorite Northwest Africa 4472: A KREEPy regolith breccia from the Moon. *Geochim. Cosmochim. Acta* **75**, 2420–2452.

Joy K. H., Crawford I. A., Anand M., Greenwood R. C., Franchi I. A. and Russell S. S. (2008) The petrology and geochemistry of Miller Range 05035: A new lunar gabbroic meteorite. *Geochim. Cosmochim. Acta* **72**, 3822–3844.

Kato C. and Moynier F. (2017) Gallium isotopic evidence for extensive volatile loss from the Moon during its formation. *Sci. Adv.* **3**, e1700571.

Kato C., Moynier F., Valdes M. C., Dhaliwal J. K. and Day J. M. D. (2015) Extensive volatile loss during formation and differentiation of the Moon. *Nat. Commun.* **6**, 1–4.

Kaufmann R., Long A., Bentley H. and Davis S. (1984) Natural Chlorine Isotope Variations. *Nature* **309**, 338–340.

Korotev R. L., Zeigler R. A., Jolliff B. L., Irving A. J. and Bunch T. E. (2009) Compositional and lithological diversity among brecciated lunar meteorites of intermediate iron concentration. *Meteorit. Planet. Sci.* **44**, 1287–1322.

Krogstad E. J. and Walker R. J. (1994) High closure temperatures of the U-Pb system in

large apatites from the Tin Mountain pegmatite, Black Hills, South Dakota, USA. *Geochim. Cosmochim. Acta* **58**, 3845–3853.

Kushiro I. and Haramura H. (1971) Major Element Variation and Possible Source Materials of Apollo 12 Crystalline Rocks. *Source Sci. New Ser.* **171**, 1235–1237. Available at: http://www.jstor.org/stable/1731185 [Accessed June 5, 2017].

Lewis J. A. and Jones R. H. (2016) Phosphate and feldspar mineralogy of equilibrated L chondrites: The record of metasomatism during metamorphism in ordinary chondrite parent bodies. *Meteorit. Planet. Sci.* **51**, 1886–1913.

Li H. and Hermann J. (2015) Apatite as an indicator of fluid salinity: An experimental study of chlorine and fluorine partitioning in subducted sediments. *Geochim. Cosmochim. Acta* **166**, 267–297.

Li H. and Hermann J. (2017) Chlorine and fluorine partitioning between apatite and sediment melt at 2.5 GPa, 800 °C: A new experimentally derived thermodynamic model. *Am. Mineral.* **102**, 580–594.

Liu Y., Floss C., Day J. M. D., Hill E. and Taylor L. A. (2009) Petrogenesis of lunar mare basalt meteorite Miller Range 05035. *Meteorit. Planet. Sci.* **44**, 261–284.

McConnell D. (1973) *Apatite. Its Crystal Chemistry, Mineralogy, Utilization, and Geologic and Biologic Occurrences.* First., Springer-Verlag.

McCubbin F. M., Boyce J. W., Srinivasan P., Santos A. R., Elardo S. M., Filiberto J., Steele A. and Shearer C. K. (2016) Heterogeneous distribution of H2O in the Martian interior: Implications for the abundance of H2O in depleted and enriched mantle sources. *Meteorit. Planet. Sci.*, 1–25.

McCubbin F. M., Elardo S. M., Shearer C. K., Smirnov A., Hauri E. H. and Draper D. S. (2013) A petrogenetic model for the comagmatic origin of chassignites and nakhlites: Inferences from chlorine-rich minerals, petrology, and geochemistry. *Meteorit. Planet. Sci.* **48**, 819–853.

McCubbin F. M., Hauri E. H., Elardo S. M., Vander Kaaden K. E., Wang J. and Shearer C. K. (2012) Hydrous melting of the martian mantle produced both depleted and enriched shergottites. *Geology* **40**, 683–686.

McCubbin F. M., Jolliff B. L., Nekvasil H., Carpenter P. K., Zeigler R. A., Steele A., Elardo S. M. and Lindsley D. H. (2011) Fluorine and chlorine abundances in lunar apatite: Implications for heterogeneous distributions of magmatic volatiles in the lunar interior. *Geochim. Cosmochim. Acta* **75**, 5073–5093.

McCubbin F. M. and Jones R. H. (2015) Extraterrestrial Apatite: Planetary Geochemistry to Astrobiology. *Elements* **11**, 183–188.

McCubbin F. M., Vander Kaaden K. E., Tartèse R., Boyce J. W., Mikhail S., Whitson E. S., Bell A. S., Anand M., Franchi I. A., Wang J. and Hauri E. H. (2015a) Experimental investigation of F, Cl, and OH partitioning between apatite and Fe-rich basaltic melt at 1.0-1.2 GPa and 950-1000 oC. *Am. Mineral.* **100**, 1790–1802.

McCubbin F. M., Vander Kaaden K. E., Tartèse R., Klima R. L., Liu Y., Mortimer J., Barnes J. J., Shearer C. K., Treiman A. H., Lawrence D. J., Elardo S. M., Hurley D. M., Boyce J. W. and Anand M. (2015b) Magmatic volatiles (H, C, N, F, S, Cl) in the lunar mantle, crust, and regolith: Abundances, distributions, processes, and reservoirs. *Am. Mineral.* **100**, 1688–1707.

McCubbin F. M., Steele A., Hauri E. H., Nekvasil H., Yamashita S. and Hemley R. J. (2010a) Nominally hydrous magmatism on the Moon. *Proc. Natl. Acad. Sci.* **107**, 11223–11228.

McCubbin F. M., Steele A., Nekvasil H., Schnieders A., Rose T., Fries M., Carpenter P. K. and Jolliff B. L. (2010b) Detection of structurally bound hydroxyl in fluorapatite from Apollo Mare basalt 15058,128 using TOF-SIMS. *Am. Mineral.* **95**, 1141–1150.

Mccubbin F. M. and Ustunisik G. (2018) Experimental investigation of F and Cl partitioning between apatite and Fe-rich basaltic melt at 0 GPa and 950-1050 oC: Evidence for steric controls on apatite-melt exchange equilibria in OH-poor apatite. *Am. Mineral.* **In press**.

Mckay D. S., Clanton U. S. and Ladle G. (1973a) Scanning electron microscope study of Apollo 15 green glass. In *4th Lunar Science Conference* pp. 225–238.

Mckay D. S., Clanton U. S. and Ladle G. (1973b) Surface morphology of Apollo 15 green glass spheres. In *4th Lunar Science Conference* pp. 484–486.

Merlivat L., Lelu M., Nief G. and Roth E. (1976) Spallation deuterium in rock 70215. In *Proceedings 7th Lunar Science Conferece* pp. 649–658.

Meyer C. (2009) Lunar Sample Compendium. *Astromaterials Res. Explor. Sci. (ARES), NASA Johnson Sp. Center, Houston, TX*. Available at: https://curator.jsc.nasa.gov/lunar/lsc/index.cfm.

Mittlefehldt D. W., Mccoy T. J., Goodrich C. A. and Kracher A. (1998) Non-chondritic meteorites from asteroidal bodies. *Planet. Mater.* **36**, 4-001-4–196.

Neal C. R. and Kramer G. Y. (2006) The petrogenesis of the Apollo 14 high-Al mare basalts. *Am. Mineral.* **91**, 1521–1535.

Neal C. R. and Taylor L. A. (1992) Petrogenesis of mare basalts: A record of lunar volcanism. *Geochim. Cosmochim. Acta* **56**, 2177–2211.

Nyquist L. E., Shih C.-Y. and Reese Y. D. (2007) Sm-Nd and Rb-Sr ages for MIL 05035: Implications for surface and mantle sources. In *38th Lunar and Planetary Sceince Conference* p. 1702.

Papike J. J., Taylor L. A. and Simon S. (1991) Lunar Minerals. In *Lunar Sourcebook: A user's guide to the Moon* (eds. G. H. Heiken, D. T. Vaniman, and B. M. French).

Patiño Douce A. E. and Roden M. (2006) Apatite as a probe of halogen and water fugacities in the terrestrial planets. *Geochim. Cosmochim. Acta* **70**, 3173–3196.

Pernet-Fisher J. F., Howarth G. H., Liu Y., Chen Y. and Taylor L. A. (2014) Estimating the lunar mantle water budget from phosphates: Complications associated with silicate-liquid-immiscibility. *Geochim. Cosmochim. Acta* **144**, 326–341.

Potts N. J., Barnes J. J., Tartèse R., Franchi I. A. and Anand M. (2018) Chlorine isotopic compositions of apatite in Apollo 14 rocks: Evidence for widespread vapor-phase metasomatism on the lunar nearside ~4 billion years ago. *Geochim. Cosmochim. Acta* **230**, 46–59. Available at: http://linkinghub.elsevier.com/retrieve/pii/S0016703718301820.

Riker J., Humphreys M. C. S., Brooker R. A., De Hoog J. C. M. and EIMF (2018) First measurements of OH-C and temperature-dependent partitioning of OH and halogens in the system apatite-silicate melt. *Am. Mineral.* **103**, 260–270.

Robinson K. L., Barnes J. J., Nagashima K., Thomen A., Franchi I. A., Huss G. R., Anand M. and Taylor G. J. (2016) Water in evolved lunar rocks: Evidence for multiple reservoirs. *Geochim. Cosmochim. Acta* **188**, 244–260. Available at: http://www.sciencedirect.com/science/article/pii/S0016703716302733 [Accessed June 2, 2017].

Rutherford M. J. and Papale P. (2009) Origin of basalt fire-fountain eruptions on Earth versus the Moon. *Geology* **37**, 219–222.

Saal A. E., Hauri E. H., Cascio M. L., Van Orman J. A., Rutherford M. C. and Cooper R. F. (2008) Volatile content of lunar volcanic glasses and the presence of water in the Moon's interior. *Nature* **454**, 192–195.

Saal A. E., Hauri E. H., Van Orman J. A. and Rutherford M. J. (2013) Hydrogen Isotopes in Lunar Volcanic Glasses and Melt Inclusions Reveal a Carbonaceous Chondrite Heritage. *Science (80-.).* **340**, 1317–1320.

Sarafian A. R., John T., Roszjar J. and Whitehouse M. J. (2017) Chlorine and hydrogen degassing in Vesta's magma ocean. *Earth Planet. Sci. Lett.* **459**, 311–319. Available at: http://dx.doi.org/10.1016/j.epsl.2016.10.029.

Sarafian A. R., Roden M. F. and Patino-Douce A. E. (2013) The volatile content of Vesta: Clues from apatite in eucrites. *Meteorit. Planet. Sci.*, 1–20.

Sato M. (1979) The driving mechanism for lunar pyroclastic eruptions inferred from the oxygen fugacity behavior of Apollo 17 orange glass. In *10th Lunar and Planetary Science Conference* pp. 311–325.

Schnare D. W., Day J. M. D., Norman M. D., Liu Y. and Taylor L. A. (2008) A laser-ablation ICP-MS study of Apollo 15 low-titanium olivine-normative and quartz-normative mare basalts. *Geochim. Cosmochim. Acta* **72**, 2556–2572. Available at: http://ac.els-cdn.com/S0016703708001105/1-s2.0-S0016703708001105-main.pdf?_tid=96ba8084-4a3f-11e7-bf33-00000aab0f6c&acdnat=1496702443_77472ec6082a54b4677fe8b9e94ca33e [Accessed June 5, 2017].

Sharp Z. D., Barnes J. D., Brearley A. J., Chaussidon M., Fischer T. P. and Kamenetsky V. S. (2007) Chlorine isotope homogeneity of the mantle, crust and carbonaceous chondrites. *Nature* **446**, 1062–1065.

Sharp Z. D., McCubbin F. M. and Shearer C. K. (2013a) A hydrogen-based oxidation mechanism relevant to planetary formation. *Earth Planet. Sci. Lett.* **380**, 88–97.

Sharp Z. D., Mercer J. A., Jones R. H., Brearley A. J., Selverstone J., Bekker A. and Stachel T. (2013b) The chlorine isotope composition of chondrites and Earth. *Geochim. Cosmochim. Acta* **107**, 189–204.

Sharp Z. D., Shearer C. K., McKeegan K. D., Barnes J. D. and Wang Y. Q. (2010) The Chlorine Isotope Composition of the Moon and Implications for an Anhydrous Mantle. *Science (80-.).* **329**, 1050–1053.

Sharp Z., Williams J., Shearer C., Agee C. and McKeegan K. (2016) The chlorine isotope composition of Martian meteorites 2. Implications for the early solar system and the formation of Mars. *Meteorit. Planet. Sci.* **51**, 2111–2126.

Shearer C. K., Messenger S. R., Sharp Z. D., Burger P. V., Nguyen A. and Mccubbin F. M. (2018) Distinct chlorine isotopic reservoirs on Mars. Implications for character, extent

and relative timing of crustal interactions with mantle-derived magmas, evolution of the martian atmosphere, and the building blocks of an early Mars. *Geochim. Cosmochim. Acta* **234**, 24–36.

Shearer C. K., Sharp Z. D., Burger P. V., McCubbin F. M., Provencio P. P., Brearley A. J. and Steele A. (2014) Chlorine distribution and its isotopic composition in “rusty rock” 66095. Implications for volatile element enrichments of “rusty rock” and lunar soils, origin of “rusty” alteration, and volatile element behavior on the Moon. *Geochim. Cosmochim. Acta*.

Shih C.-Y., Nyquist L. E., Reese Y. and Bischoff A. (2008) Sm-Nd and Rb-Sr isotopic studies of meteorite Kalahari 009: An old VLT mare basalt. In *39th Lunar and Planetary Science Conference*

Smith J. ., Anderson A. T., Newton R. C., Olsen E. J. and Wyllie P. J. (1970) Petrologic history of the moon inferred from petrography, mineralogy and petrogenesis of Apollo 11 rocks. *Geochim. Cosmochim. Acta Suppl. 1* **1**, 897–925.

Snape J. F., Curran N. M., Whitehouse M. J., Nemchin A. A., Joy K. H., Hopkinson T., Anand M., Bellucci J. J. and Kenny G. G. (2018) Ancient volcanism on the Moon: Insights from Pb isotopes in the MIL 13317 and Kalahari 009 lunar meteorites. *Earth Planet. Sci. Lett.* **502**, 84–95. Available at: https://doi.org/10.1016/j.epsl.2018.08.035.

Snape J. F., Nemchin A. A., Bellucci J. J., Whitehouse M. J., Tartèse R., Barnes J. J., Anand M., Crawford I. A. and Joy K. H. (2016) Lunar basalt chronology, mantle differentiation and implications for determining the age of the Moon. *Earth Planet. Sci. Lett.* **451**, 149–158.

Snyder G. A., Borg L. E., Nyquist L. E. and Taylor L. A. (2000) Chronology and isotopic constraints on lunar evolution. In *Origin of the Earth and Moon* (eds. R. M. Canup and K. Righter). University of Arizona Press. pp. 361–396.

Sokol A. K., Fernandes V. A., Schulz T., Bischoff A., Burgess R., Clayton R. N., Münker C., Nishiizumi K., Palme H., Schultz L., Weckwerth G., Mezger K. and Horstmann M. (2008) Geochemistry, petrology and ages of the lunar meteorites Kalahari 008 and 009: New constraints on early lunar evolution. *Geochim. Cosmochim. Acta* **72**, 4845–4873.

Tartèse R. and Anand M. (2013) Late delivery of chondritic hydrogen into the lunar mantle: Insights from mare basalts. *Earth Planet. Sci. Lett.* **361**, 480–486.

Tartèse R., Anand M., Barnes J. J., Starkey N. A., Franchi I. A. and Sano Y. (2013) The abundance, distribution, and isotopic composition of Hydrogen in the Moon as revealed by basaltic lunar samples: Implications for the volatile inventory of the Moon. *Geochim. Cosmochim. Acta* **122**, 58–74.

Tartèse R., Anand M., Joy K. H. and Franchi I. A. (2014a) H and Cl isotope systematics of apatite in brecciated lunar meteorites Northwest Africa 4472, Northwest Africa 773, Sayh al Uhaymir 169, and Kalahari 009. *Meteorit. Planet. Sci.* **49**, 2266–2289.

Tartèse R., Anand M., McCubbin F. M., Elardo S. M., Shearer C. K. and Franchi I. A. (2014b) Apatites in lunar KREEP basalts: The missing link to understanding the H isotope systematics of the Moon. *Geology* **42**, 363–366.

Terada K., Anand M., Sokol A. K., Bischoff A. and Sano Y. (2007) Cryptomare magmatism 4.35 Gyr ago recorded in lunar meteorite Kalahari 009. *Nature* **450**, 849–853.

Treiman A. H., Boyce J. W., Greenwood J. P., Eiler J. M., Gross J., Guan Y., Ma C. and

Stolper E. M. (2016) D-poor hydrogen in lunar mare basalts assimilated from lunar regolith. *Am. Mineral.* **101**, 1596–1603.

Treiman A. H., Boyce J. W., Gross J., Guan Y., Eiler J. M. and Stolper E. M. (2014) Phosphate-halogen metasomatism of lunar granulite 79215: Impact-induced fractionation of volatiles and incompatible elements. *Am. Mineral.* **99**, 1860–1870. Available at: http://ammin.geoscienceworld.org/content/99/10/1860 [Accessed June 2, 2017].

Ustunisik G., Nekvasil H. and Lindsley D. (2011) Differential degassing of H2O, Cl, F, and S: Potential effects on lunar apatite. *Am. Mineral.* **96**, 1650–1653.

Ustunisik G., Nekvasil H., Lindsley D. H. and McCubbin F. M. (2015) Degassing pathways of Cl-, F-, H-, and S-bearing magmas near the lunar surface: Implications for the composition and Cl isotopic values of lunar apatite. *Am. Mineral.* **100**, 1717–1727.

Wang Y., Guan Y., Hsu W. and Eiler J. M. (2012) Water content, chlorine and hydrogen isotope compositions of lunar apatite. In *Meteoritical Society Meeting* p. 5170.

Warren P. H. and Wasson J. T. (1979) The origin of KREEP. *Rev. Geophys. Sp. Phys.* **17**, 73–88.

Wetzel D. T., Hauri E. H., Saal A. E. and Rutherford M. J. (2015) Carbon content and degassing history of the lunar volcanic glasses. *Nat. Geosci.* **8**, 755–758.

Wetzel D. T., Rutherford M. J., Jacobsen S. D., Hauri E. H. and Saal A. E. (2013) Degassing of reduced carbon from planetary basalts. *Proc. Natl. Acad. Sci.* **110**, 8010–8013.

Williams J. T., Shearer C. K., Sharp Z. D., Burger P. V., McCubbin F. M., Santos A. R., Agee C. B. and McKeegan K. D. (2016) The chlorine isotopic composition of Martian meteorites 1: Chlorine isotope composition of Martian mantle and crustal reservoirs and their interactions. *Meteorit. Planet. Sci.* **51**, 2092–2110.

Wood J. A., Dickey J. S. J., Marvin U. B. and Powell B. N. (1970) Lunar anorthosites and a geophysical model of the Moon. *Geochim. Cosmochim. Acta Suppl. 1* **1**, 965–988. Available at: http://articles.adsabs.harvard.edu/cgi-bin/nph-iarticle_query?1970gecas...1..965w&defaultprint=YES&filetype=.pdf [Accessed June 7, 2017].

Zhang A.-C., Hsu W. B., Floss C., Li X. H., Li Q. L., Liu Y. and Taylor L. A. (2011) Petrogenesis of lunar meteorite Northwest Africa 2977: Constraints from in situ microprobe results. *Meteorit. Planet. Sci.* **45**, 1929–1947.

Table 1. Cl isotope and volatile abundance (Cl and H_2O equivalent) data obtained simultaneously on apatite in the lunar samples studied. B.d. below detection, n.m. not measured. * Background H_2O measured on the blank contributed more than 50% to the measured H_2O value. Note that 'Kal2_Ap4a' was measured in a different thin section to the other three Kalahari 009 analyses

Sample ID	δ^{37}Cl (‰)	2s (‰)	H_2O (ppm)	2s (ppm)	F (wt%)	2s (wt%)	Cl (wt%)	2s (ppm)	H_2O blank (ppm)	% blank (ppm)
12064 Ap4a	14.9	1.5	473	18	2.87	0.30	0.20	35	275	37
12064 Ap4b	12.9	1.4	824	31	2.94	0.31	0.24	41	275	25
12064 Ap2a	13.0	3.2	715	27	3.08	0.32	0.04	7	275	28
12064 Ap2b	13.9	2.8	1378	51	2.85	0.30	0.06	21	275	17
12064 Ap1a	10.3	3.0	930	34	3.10	0.32	0.05	16	275	23
12064 Ap1b	11.2	1.6	2347	87	2.77	0.29	0.21	75	275	10
12039 Ap9a	13.6	3.0	1589	155	3.22	0.15	0.05	7	144	8
12039 Ap9b	15.1	2.9	1471	143	3.21	0.15	0.05	8	144	9
12039 Ap11a	15.4	2.8	2395	234	2.57	0.12	0.06	9	144	6
12039 Ap8a	15.3	2.0	1638	160	2.87	0.14	0.13	19	144	8
12039 Ap1a	16.5	1.5	3735	364	2.21	0.11	0.26	37	144	4
12039 Ap1b	19.4	2.6	1675	163	2.49	0.12	0.07	10	144	8
12039 Ap2a	15.5	2.3	1839	179	2.96	0.14	0.09	13	144	7
15016 Ap25a	14.0	2.6	64	5	3.69	0.36	0.09	37	40	39
15016 Ap9b *	13.3	1.6	38	4	2.89	0.14	0.31	162	144	79
15016 Ap31b	9.9	5.1	b.d.	b.d.	3.38	0.16	0.01	8	144	-
15016 Ap11a	12.8	2.5	342	33	3.16	0.15	0.08	40	144	30
15016 Ap6a	11.0	2.7	b.d.	b.d.	3.20	0.15	0.06	33	144	-
15058 Ap1a *	9.1	1.5	210	8	3.24	0.34	0.27	95	275	57
15058 Ap2 *	10.7	1.2	273	10	2.90	0.30	0.48	173	275	50
15058 Ap4	7.4	1.6	554	21	2.91	0.30	0.29	103	275	33
15058 Ap5 *	12.2	1.4	94	3	2.91	0.30	0.36	129	275	75
15058 Ap5b *	8.2	1.8	164	6	3.47	0.36	0.16	59	275	63
Table 1 continued										
Sample ID	**δ^{37}Cl (‰)**	**2s (‰)**	**H_2O (ppm)**	**2s (ppm)**	**F (wt%)**	**2s (wt%)**	**Cl (wt%)**	**2s (ppm)**	**H_2O blank (ppm)**	**% blank (ppm)**
15065 Ap10a	9.2	1.1	2786	103	2.25	0.23	0.44	75	275	9
15065 Ap10b	12.0	1.1	2273	84	2.17	0.23	0.40	68	275	11
15065 Ap11a	10.1	1.9	2220	82	2.53	0.26	0.12	20	275	11
15065 Ap12	10.3	1.7	2097	78	2.57	0.27	0.14	25	275	12
15065 Ap13	10.2	1.7	2562	95	2.40	0.25	0.16	28	275	10
70017 Ap1a *	15.3	2.3	42	2	3.30	0.34	0.08	28	275	87
70017 Ap1b *	11.7	2.3	7	<1	3.35	0.35	0.07	26	275	98
70017 Ap12 *	14.9	1.5	3	<1	3.47	0.36	0.07	24	275	99
70017 Ap3 *	16.8	2.1	21	1	3.54	0.37	0.08	29	275	93
70017 Ap4	9.1	0.6	b.d.	b.d.	3.37	0.35	1.36	486	275	-

MIL05035 Ap11B2	3.6	1.3	n.m.	n.m.	n.m.	n.m.	0.66	181	-	-
MIL05035 Ap11C	7.1	1.3	n.m.	n.m.	n.m.	n.m.	0.70	192	-	-
MIL05035 Ap11D	5.2	1.4	2900	123	2.98	0.29	0.82	287	643	18
MIL05035 Ap1	7.5	1.4	2277	96	2.39	0.23	0.95	331	643	22
Kal009 Ap2	22.0	2.7	b.d.	b.d.	3.43	0.33	0.08	37	643	-
Kal009 Ap2b	22.4	2.4	b.d.	b.d.	3.35	0.33	0.08	36	643	-
Kal009 Ap1	15.4	1.4	b.d.	b.d.	3.40	0.33	0.49	235	643	-
Kal2 Ap4a	15.6	0.9	1302	103	n.m.	n.m.	0.45	227	105	7

Table 2. H_2O content and corresponding hydrogen isotope data for apatite in 15016 and 15065. The H_2O content and δD values have been corrected for contribution from instrumental background and the D/H of the background. The data shown have been corrected for the effects of H and D produced by cosmic ray spallation using two production rates for D (for further details the reader is referred to the electronic annex).

	Background corrected				**Spallation corrected[a]: P_D =4.6 ×10^{-13}**					**Spallation corrected[b]: P_D =2.17±0.11 ×10^{-12}**				
Analysis ID	**H_2O (ppm)**	**2s (ppm)**	**δD (‰)**	**2s (‰)**	**H_2O (ppm)**	**2s (ppm)**	**δD (‰)**	**2s + (‰)**	**2s - (‰)**	**H_2O (ppm)**	**2s (ppm)**	**δD (‰)**	**2s + (‰)**	**2s - (‰)**
15016_Ap25a	379	50	-36	104	377	50	-83	107	110	377	50	-152	106	108
15016_Ap6a	184	25	200	131	183	25	103	142	149	183	25	-40	139	144
15016_Ap31a	90	13	262	174	89	13	65	209	230	89	13	-229	199	213
15016_Ap31a	77	12	295	188	75	12	63	232	259	75	12	-283	221	237
15016_Ap42a	55	9	806	245	54	9	494	306	345	54	9	11	291	320
15016_Ap11a	350	46	380	206	348	46	330	208	209	348	46	255	207	208
15065_Ap14a	2887	367	976	35	2886	367	970	35	35	2886	367	961	35	35
15065_15a	1817	232	1087	39	1815	232	1078	39	40	1815	232	1063	39	40
15065_Ap12a	2657	338	997	36	2655	338	991	36	36	2655	338	981	36	36
15065_Ap12b	2730	347	938	36	2728	347	932	36	36	2728	347	922	36	36

Where: [a]Production rate of deuterium from Merlivat et al. (1976) ~4.6x10^{-13} mol(g rock)$^{-1}$ Ma^{-1}. [b]Production rate of de (2017) 2.17x10^{-12} mol(g rock)$^{-1}$ Ma^{-1}. The average reported cosmic ray exposure age for 15016 (362 ± 59 Ma, Füri et al 2018) was used to correct both 15016 and 15065 data as no exposure age information is available for 15065.